

HUMBOLDT-UNIVERSITÄT ZU BERLIN
MATHEMATISCH-NATURWISSENSCHAFTLICHE FAKULTÄT
INSTITUT FÜR PHYSIK

Asymptotic behavior of a generalized Lévy walk model

Masterarbeit

zur Erlangung des akademischen Grades
Master of Science (M. Sc.)

eingereicht von: Marius Bothe

geboren am: 23.2.1995

geboren in: Bonn

Gutachter/innen: Prof. Dr. Igor Sokolov
Dr. habil. Michael Zaks

eingereicht am: verteidigt am:

Contents

1. Introduction	1
2. Theoretical Background	3
2.1. The model	3
2.1.1. Lévy walks	3
2.1.2. Generalized Lévy walks	5
2.2. Theory of random walks	8
2.2.1. Transport equation for the PDF in the ordinary case	8
2.2.2. Transport equation for the PDF in the aged case	11
2.2.3. Forward waiting time and step rate	12
3. Methods	14
3.1. Method for calculating the MSD	14
3.2. Method for calculating the PDF	16
3.3. Numerical simulation of the model	17
4. Analytical Calculations	19
4.1. MSD in the ordinary case	19
4.2. MSD in the aged case: general expressions	27
4.3. MSD in the aged case: short aging times	28
4.4. MSD in the aged case: long aging times	34
4.5. PDF in the ordinary case	39
5. Results and Discussion	43
5.1. Ordinary MSD	43
5.2. Aged MSD	45
5.3. Simulation of the PDF in the ordinary case	48
5.4. Simulation of the PDF in the aged case	54
5.5. Probability density at the origin	58
5.6. Analytic results for the PDF	59
6. Conclusions	62
A. The Tauberian theorem	64
B. Estimates for the integral $I_{a,b,c}(y)$	67

1. Introduction

Experimental results show, that a variety of diffusive systems display behavior that can not be explained by normal diffusion, because for these processes the mean squared displacement (MSD) does not grow linearly with time [1–4] . Models that can capture and describe this anomalous behavior are therefore of great interest, and continuous time random walk (CTRW) models with power law step distributions turned out to be particularly suitable for this task.

One such model is the Lévy walk, which had considerable success by introducing a space-time coupling, which fixed many of the divergence issues that plagued the model's predecessors, namely the related Lévy flights. It was first presented in [5] as a way to describe the anomalous diffusion in the atmosphere found by Richardson [6]. The model has since been used to describe a variety of processes [7] , such as the movement of cold atoms in an optical lattice [8], the statistics of blinking quantum dots [9], the spread of perturbations in a many-particle Hamiltonian system [10] and the movement of E. coli bacteria [11].

Lévy walks are a special kind of isotropic CTRW, where the walker does not wait at the change points, but the waiting time is instead moved into the steps, which no longer happen instantaneously but have a finite duration. This step duration is coupled to the length of the step and follows a power law distribution $\psi(t) \propto t^{-\gamma-1}$, whose tail is determined by the parameter $\gamma > 0$.

There are multiple variations of the model, which connect step duration and length in different ways: For example in the so-called velocity model the speed of the walker is a constant, $v = c$. However the original model proposed in [5] has a more general space-time coupling, where the fixed speed in a step of total duration t is given by $v = ct^{\nu-1}$, such that the displacement in a completed step is $|\mathbf{x}_i| = ct^{\nu}$, where the parameter ν governs the speed's dependence on the step's duration. This way the model was thought to be able to describe various kinds of anomalous diffusion for different values of the parameters γ and ν , including the so-called Richardson regime, which is characterized by a cubic time dependence of the MSD, $\langle \mathbf{x}^2 \rangle \propto t^3$.

But the model's ability to describe these regimes was called into question in a recent publication [12] , where it was found that the MSD is divergent for certain relations of the parameters γ and ν , including in the region where the Richardson regime was thought to appear. This divergence had gone unnoticed during the three decades since

the invention of the model and poses a serious problem, especially considering that the space-time coupling had mainly been introduced to fix the divergent MSDs of previous models.

So how can this divergence be remedied? The main issue of the original model is, that the walker adopts his full speed right at the beginning of the step, and this speed grows with the total step duration, which is not bounded by the observation time. Therefore a natural solution is to study models that have a more gradual acceleration. Such models have been considered in [13, 14], where a variation of the Lévy walk was investigated that is closer to the Drude model for conduction in solids.

However in the supplementary material of [12] a generalized Lévy walk model is presented, which introduces a third parameter, η , that allows interpolation between the original model and the Drude-like model. The authors of [12] show for the ordinary (non aged) case that this new parameter allows for finite MSD in the parameter region where the Richardson regime is suspected, but they do not explicitly calculate the MSD in the new model.

This thesis therefore investigates this new, generalized model. To this end the behavior of the MSD in one dimension is calculated for arbitrary η , both in the ordinary as well as in the aged case, which is published in [15]. The aim here is to provide finite predictions for the MSD, which is well measurable and can connect the model to experimental results. Furthermore the effects of η on the probability distribution function (PDF) are analyzed.

2. Theoretical Background

2.1. The model

2.1.1. Lévy walks

The original motivation for the invention of the Lévy walk model goes back to the work of Richardson [6], who studied the motion of particles in the turbulent flow of the atmosphere. Such a system contains jets and eddies, which affect the behavior of the particle and lead to anomalous diffusion¹, namely the Richardson regime of $\langle \mathbf{x}^2 \rangle(t) \propto t^3$.

Power law distributions proved themselves to be particularly suitable for describing anomalous diffusion, which lead to the invention of the Lévy flight: Similar to the Lévy walk the particle moves isotropically, but the jumps happen instantaneously, with a jump length drawn from a distribution $g(|\mathbf{x}|)$. After reaching the change point the walker waits for the duration of the waiting time, which is drawn from the independent distribution $\psi(t)$, and then performs the next jump. Both the waiting time and the jump length distributions are power laws, meaning for large arguments they take the form

$$\psi(t) \propto t^{-1-\gamma}, \quad g(|\mathbf{x}|) \propto |\mathbf{x}|^{-1-\beta}, \quad \gamma, \beta > 0. \quad (2.1)$$

However the Lévy flight model has a major drawback: Since the jumps happen instantaneously, it has an infinite propagation speed, which causes its MSD and all higher moments to diverge [7].

Therefore the Lévy walk model was developed by Shlesinger, Klafter and West [5]: Here the walker no longer waits at the change points, and instead of jumps the walker performs steps, which have a finite duration. This step duration is coupled to the length of the step and prevents the infinite propagation speed that caused problems with the Lévy flights. The two walks are contrasted in Fig. 2.1.

¹There are different kinds of anomalous diffusion: A process with $\langle \mathbf{x}^2 \rangle(t) \propto t^\alpha$ is called subdiffusive for $\alpha < 1$, normal for $\alpha = 1$, superdiffusive for $1 < \alpha < 2$, ballistic for $\alpha = 2$ and superballistic for $\alpha > 2$. The Richardson regime is therefore a special case of superballistic diffusion.

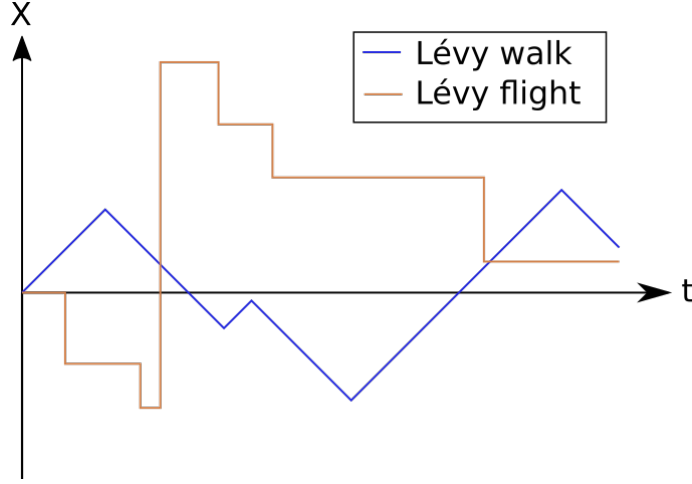


Figure 2.1.: Comparison between the trajectories of the one dimensional Lévy flight and Lévy walk (for $\nu = 1$). Note that the jump length of the Lévy flight is independent of the waiting time.

The path of a walker in the new model is now described by a series of step durations, t_1, t_2, \dots , which are drawn from the power law distribution

$$\psi(t) = \frac{\gamma}{t_0} \frac{1}{(1 + t/t_0)^{\gamma+1}}. \quad (2.2)$$

Here the parameter $\gamma > 0$ governs the width of the distribution and t_0 is the typical timescale of a step. These step durations are associated with their respective displacements, $\mathbf{x}_1, \mathbf{x}_2, \dots$, whose direction is chosen randomly. By partially summing up the step durations and the step lengths one obtains the change times T_n and the change points \mathbf{X}_n respectively:

$$T_n = \sum_{j=1}^n t_j, \quad \mathbf{X}_n = \sum_{j=1}^n \mathbf{x}_j. \quad (2.3)$$

Now consider the walker at the observation time t : We denote the last change time by $T_n = \max\{T_i | T_i \leq t\}$, so that the distance covered in the last step is given by

$$|\mathbf{x}_{n+1}| = c(t_{n+1})^{\nu-1}(t - T_n), \quad (2.4)$$

where c is a constant with dimension $[L][T]^{-\nu}$. The speed,

$$v = \frac{\partial}{\partial t} |\mathbf{x}_{n+1}| = c(t_{n+1})^{\nu-1}, \quad (2.5)$$

is therefore fixed during the entire step but depends on the total step duration t_{n+1} , and the parameter $\nu > 0$ governs this dependence. For any completed step we can now

write down the joint probability to make a step with displacement \mathbf{x} and duration t :

$$\psi(\mathbf{x}, t) = \frac{\gamma}{t_0} \frac{1}{(1 + t/t_0)^{\gamma+1}} \frac{\delta(|\mathbf{x}| - ct^\nu)}{|\mathbf{x}|^{d-1} |S^{d-1}|}. \quad (2.6)$$

Here d is the spatial dimension of the process, and $|S^{d-1}|$ is the surface area of a d -dimensional unit ball, which is added for normalization. Note that both the distribution of step durations and the joint distribution are denoted by ψ , but can be distinguished by their arguments.

In conclusion we have a model that is governed by two parameters, ν and γ , and can produce different kinds of anomalous diffusion.

However it was recently discovered in [12] that the MSD of the model is actually divergent for certain values of its parameters. This divergence was found by writing down the contribution to the second moment from the trajectories that consist of a single step longer than the observation time, i.e. the cases where the walker never stops during observation:

$$\langle \mathbf{x}^2 \rangle(t) \geq \int_{\mathbb{R}^d} \int_t^\infty |\mathbf{x}|^2 \psi(\mathbf{x}, t') dt' d^d x \quad (2.7)$$

$$= \frac{\gamma}{t_0} \int_0^\infty \int_t^\infty |\mathbf{x}|^2 \frac{1}{(1 + t'/t_0)^{\gamma+1}} \delta(|\mathbf{x}| - c(t')^{\nu-1}t) dt' d|\mathbf{x}| \quad (2.8)$$

$$= \frac{\gamma t^2}{t_0} \int_t^\infty \frac{c^2(t')^{2\nu-2}}{(1 + t'/t_0)^{\gamma+1}} dt'. \quad (2.9)$$

The integrand is proportional to $(t')^{2\nu-\gamma-3}$, therefore the integral will diverge at infinity whenever $2\nu \geq \gamma + 2$ holds. This includes the parameter region where the Richardson regime was expected, so the model, which was essentially invented to cure the divergence in the description of the Richardson regime, turns out to be divergent itself. In order to remedy this, a more general model is necessary.

2.1.2. Generalized Lévy walks

Because very long steps that start with arbitrarily high velocities cause the divergence, a solution might be to let the particle start with a lower initial speed and compensating for the slower start by accelerating it throughout the step, so that it catches up with its constant velocity counterpart at the end of the step.

As mentioned in the introduction such an acceleration is considered in the Drude-like models in [13, 14]. This is generalized by the introduction of the acceleration parameter η in the supplementary material of [12], which interpolates between the original Lévy model and the Drude-like scheme. In the thesis we will investigate this generalized Lévy walk.

The step durations in this model are distributed as in the previous model, see Eq. (2.2), but the position between two change points is calculated differently: Instead of a linear time dependence we now have a dependence on the new parameter η for the displacement in the $(n+1)$ th step:

$$|\mathbf{x}_{n+1}| = c(t_{n+1})^{\nu-\eta}(t - T_n)^\eta. \quad (2.10)$$

Therefore the particle moves in general with a non-constant speed

$$v = c\eta(t_{n+1})^{\nu-\eta}(t - T_n)^{\eta-1}. \quad (2.11)$$

Note that this influences neither the change points nor the change times. The distribution of completed steps is therefore still given by

$$\psi(\mathbf{x}, t) = \frac{\gamma}{t_0} \frac{1}{(1 + t/t_0)^{\gamma+1}} \frac{\delta(|\mathbf{x}| - ct^\nu)}{|\mathbf{x}|^{d-1} |S^{d-1}|}. \quad (2.12)$$

However the position in between two change times now depends on η [12], which is

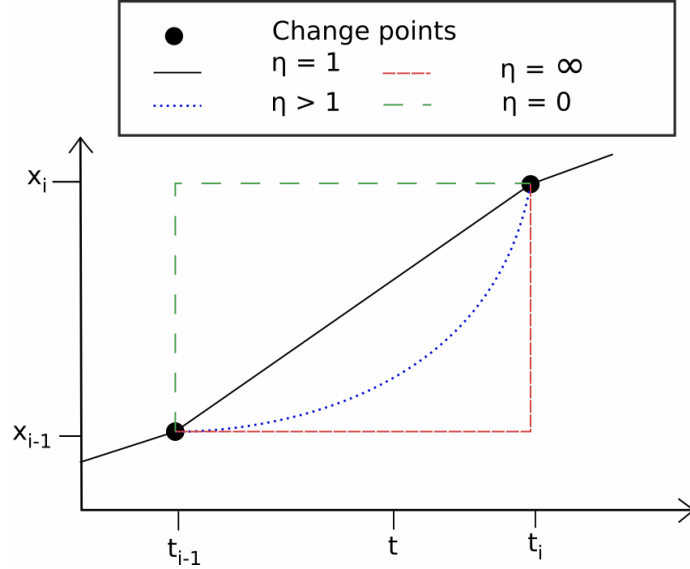


Figure 2.2.: Comparison of a walker's motion for different values of η : The trajectories and change points remain the same, but the position measured at time t varies. For $\eta = 1$ the walker moves with constant speed and has some non-linear time dependence for $\eta > 1$. In the limits $\eta = 0$ and $\eta = \infty$ we replicate the time-coupled Lévy flight, where the two limits correspond to the walker jumping first and then waiting or waiting first and then jumping.

illustrated in Fig. 2.2 (taken from [15]). This affects the last incomplete steps of the walk, which we have seen to be responsible for the divergence in the original model.

To summarize, the generalized model now depends on three parameters: ν determines how the step length of the walker depends on the step durations, η governs the acceleration in between the change points and γ describes the tail of the waiting time distribution.

The anomalous nature of Lévy walk diffusion can be understood by looking at the moments of the steps: We can directly read off from Eq. (2.2) that the mean step duration is only finite for $\gamma > 1$.

Furthermore the distribution of lengths for completed steps takes the form

$$p(|\mathbf{x}|)dx \propto |\mathbf{x}|^{-\frac{\gamma+\nu}{\nu}} dx, \quad (2.13)$$

which follows from Eq. (2.2) by using $|\mathbf{x}| = ct^\nu$. From this we can deduce that the mean squared step length diverges for $2\nu > \gamma$.

Both the average step duration and the mean squared step length are of great importance because the central limit theorem asserts that the cumulative distribution of the sum of N independent identically distributed random variables of finite variance tends towards a Gaussian as $N \rightarrow \infty$. This applies to the Lévy walk only when the mean squared step length is finite, and the number of steps actually tends to infinity, i.e. when the mean step duration does not diverge. In other words, for $\gamma > 2\nu$, $\gamma > 1$ we expect the PDF of the walk to tend towards a Gaussian in the asymptotic limit, which implies that the walker should show normal diffusive behavior with $\langle \mathbf{x}^2 \rangle \propto t$.

However outside of this parameter range the walk is no longer subject to the central limit theorem. Instead it was shown by Paul Lévy in 1920 that in this case the cumulative distribution of the sum of the variables converges to one of the so-called Lévy alpha-stable distributions, which is the statement of the generalized central limit theorem [7]. It is this close relation to Lévy distributions that gave the Lévy flights and later the Lévy walks their name. The divergence of the variance of the step length is therefore not bug, but a key feature for the modeling of anomalous diffusion.

A second important quality of the Lévy walk model in general and the generalized model in particular is, that it is a semi-Markov process. A process is considered Markov if the behavior of the walker after a point in time t only depends on its position and velocity at t , not on its history. For a CTRW, of which Lévy walks are an example, this is not the case in general [16], as information about the last step, i.e. how long the walker is already moving, is important for predicting the future behavior (with the exception of Gaussian step distributions). However in our case this memory only extends to the last previous step, and the process is renewed at every change point, which makes it semi-Markov [7].

It is therefore of great interest to understand the behavior of a walker that has started moving at $t = -t_a$ and is therefore already in the middle of a step at the beginning of observation at $t = 0$. Such an aged situation was considered for similar models in [17, 18] and is also investigated in this thesis, where we calculate the asymptotic MSD of the generalized Lévy walk in the aged case.

A third related property is the weak ergodicity breaking in Lévy walks: A process breaks ergodicity if its time averages and ensemble averages do not converge to the same value: This usually happens because the trajectory of the solution observed in the time average cannot explore the entire phase space, while the ensemble average reaches over the full phase space. However in the case of weak ergodicity breaking the particle is able to reach any point phase space, but the time to do this is on the same scale or larger than the total observation time, which means it does not converge reliably to the same value as the ensemble average.

Ergodicity breaking is of great interest for the theoretical as well as the experimental community as it determines what results we can expect from different kinds of measurements. Power law distributions as used in Lévy process are closely connected to weak ergodicity breaking, as their typical timescale for reaching a convergent average is divergent in subdiffusive regimes [19], which has been studied for example in [12, 20]. While this thesis will not investigate the ergodicity breaking of the new model explicitly, this property is connected to the behavior of the aged walk, which is considered in the calculation of the MSD.

Note that all averages throughout the thesis are understood to be ensemble averages.

2.2. Theory of random walks

In this chapter I will briefly cover some of the main results of the theory of random walks that are used in this thesis. A more detailed description can be found in [16].

2.2.1. Transport equation for the PDF in the ordinary case

We have seen that for the Lévy walk each step is determined by a joint distribution of both the step duration t and the step distance \mathbf{x} , where the coupling between space and time is introduced by one being conditioned on the other:

$$\psi(\mathbf{x}, t) = \psi(t)f(\mathbf{x}|t). \quad (2.14)$$

We are now interested in the distribution of completed steps, $C(x, t)$, which is the probability density of a particle starting at $\mathbf{x} = 0$, $t = 0$ reaching a change point at time t and position \mathbf{x} after an arbitrary number of steps in between. A transport equation can be written down for $C(\mathbf{x}, t)$ which reads [16]:

$$C(\mathbf{x}, t) = \int_{R^d} d^d \mathbf{x}' \int_0^t dt' C(\mathbf{x}', t') \psi(\mathbf{x} - \mathbf{x}', t - t') + \delta(t)\delta(\mathbf{x}). \quad (2.15)$$

The two terms on the right hand side express two different contributions to the probability of finding a change point at (\mathbf{x}, t) :

The first term is a convolution integral in \mathbf{x}' and t' . It expresses the fact that there will be a change point at (\mathbf{x}, t) exactly when there has been a change point at the primed coordinates (\mathbf{x}', t') and the walker performs a jump with displacement $\mathbf{x} - \mathbf{x}'$ and duration $t - t'$ from (\mathbf{x}', t') to (\mathbf{x}, t) .

The second term just enforces that by definition we will find the particle at the origin at the beginning of observation.

To evaluate this integral equation it is useful to go to the Fourier-Laplace domain, where the transformations are defined as follows:

The Laplace transform of a function $f(t)$ is defined as the integral

$$\mathcal{L}\{f(t), s\} = f(s) = \int_0^\infty e^{-st} f(t) dt. \quad (2.16)$$

Note that the distinction between the function and its transform is only made in the argument of the function, which is either t or s .

The Laplace transform is unique up to a set of points with Lebesgue measure zero and can be inverted via the Bromwich integral

$$\mathcal{L}^{-1}\{f(s), t\} = f(t) = \frac{1}{2\pi i} \int_{-i\infty+c}^{+i\infty+c} e^{st} f(s) ds, \quad (2.17)$$

where $c \in \mathbb{R}$ is chosen such that $f(s)$ exists on the contour.

For Fourier transforms we use the variables $\mathbf{x} \leftrightarrow \mathbf{k}$, with the distinction between the function and its transform again only being shown via the argument. They are defined by the integral

$$\mathcal{F}\{f(\mathbf{x}), \mathbf{k}\} = f(\mathbf{k}) = \int_{\mathbb{R}^d} e^{i\mathbf{k}\cdot\mathbf{x}} f(\mathbf{x}) d^d x, \quad (2.18)$$

with the inverse

$$\mathcal{F}^{-1}\{f(\mathbf{k}), \mathbf{x}\} = f(\mathbf{x}) = \frac{1}{(2\pi)^d} \int_{\mathbb{R}^d} e^{-i\mathbf{k}\cdot\mathbf{x}} f(\mathbf{k}) d^d k, \quad (2.19)$$

where the normalization factor $\frac{1}{(2\pi)^d}$ is kept in the inverse transform.

The Fourier and the Laplace transform turn convolutions of functions into simple products, a useful property that will be used frequently throughout the thesis. This means

$$\mathcal{L}\left\{\int_0^t f(t')g(t-t')dt', s\right\} = f(s)g(s), \quad (2.20)$$

and

$$\mathcal{F}\left\{\int_{\mathbb{R}^d} f(\mathbf{x}')g(\mathbf{x}-\mathbf{x}')d^d x', \mathbf{k}\right\} = f(\mathbf{k})g(\mathbf{k}). \quad (2.21)$$

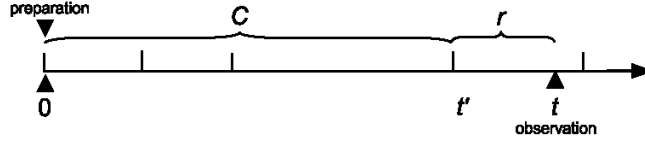


Figure 2.3.: Illustration of the path of a Lévy walker on the time axis. Each tick on the line represents a change time. The walker starts at $t = 0$ and is observed at time t during a final incomplete step described by the distribution $r(\mathbf{x}, t)$ after it has completed a series of steps, which is described by $C(\mathbf{x}, t)$.

Applying this to the convolution in Eq. (2.15) we obtain

$$C(\mathbf{k}, s) = C(\mathbf{k}, s) \psi(\mathbf{k}, s) + 1, \quad (2.22)$$

which gives us a closed expression for $C(\mathbf{k}, s)$:

$$C(\mathbf{k}, s) = \frac{1}{1 - \psi(\mathbf{k}, s)}. \quad (2.23)$$

We now want to express the probability distribution of the ordinary Lévy walk, $p(\mathbf{x}|t)$, using this result. $p(\mathbf{x}|t)$ describes the probability of finding the walker at \mathbf{x} given that it is observed at time t , where it can either be at a change point or in motion, as illustrated in Fig. 2.3. In order to write down a transport equation for $p(\mathbf{x}|t)$ we need to introduce the probability density for the rest of the walk after the last change point, denoted by $r(\mathbf{x}|t)$ ². $r(\mathbf{x}|t)$ describes the probability that a walker starts at $(\mathbf{0}, 0)$ and performs a single step of duration equal or longer than the observation time t , such that he is found at position \mathbf{x} at t . In the case of the generalized Lévy walk this can be cast into the equation

$$r(\mathbf{x}|t) = \int_t^\infty \frac{1}{|\mathbf{x}|^{d-1} |S^{d-1}|} \delta(|\mathbf{x}| - ct^\eta t'^{\nu-\eta}) \psi(t') dt'. \quad (2.24)$$

With this expression for $r(\mathbf{x}|t)$ we can now write down $p(\mathbf{x}|t)$ as a convolution of $r(\mathbf{x}|t)$ and $C(\mathbf{x}, t)$:

$$p(\mathbf{x}|t) = \int_{\mathbb{R}^d} \int_0^t C(\mathbf{x}', t') r(\mathbf{x} - \mathbf{x}'|t - t') dt' d^d x', \quad (2.25)$$

which describes a walker starting at the origin, performing a series of completed steps ending at \mathbf{x}' and then performing a final, incomplete step that leaves him at position \mathbf{x}

² Throughout the thesis I will use capital letters for probability densities that depend jointly on space and time, like $C(\mathbf{x}, t)$, and lower case letters for densities that depend only on space and are conditioned on time, like $r(\mathbf{x}|t)$. Note that the former have dimension $[L]^{-d} [T]^{-1}$, while the latter have dimension $[L]^{-d}$.

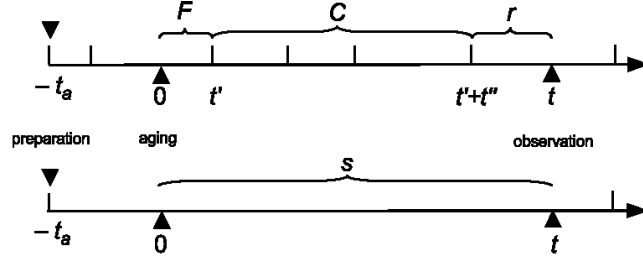


Figure 2.4.: Illustration of an aged Lévy walk on the time axis. Each tick on the line represents a change time. The walker starts at $-t_a$ and observation begins at $t = 0$. In the upper picture we see the case that the first observed change time is at $t' < t$, the probability of this event is given by F . From here walker performs a series of completed steps and a final incomplete step as in the ordinary case. The lower picture shows the case that the first change point is after the end of observation, i.e. the walker never stops during observation. The probability density of this event is given by s .

at observation time t .

We now use the convolution properties of the Fourier and the Laplace transform, equations (2.20) and (2.21), to obtain

$$p(\mathbf{k}|s) = C(\mathbf{k}, s)r(\mathbf{k}|s). \quad (2.26)$$

Substituting for $C(\mathbf{k}, s)$ with formula (2.23) yields

$$p(\mathbf{k}|s) = \frac{r(\mathbf{k}|s)}{1 - \psi(\mathbf{k}, s)}, \quad (2.27)$$

which gives us an algebraic equation for the PDF in the Fourier-Laplace domain that depends only on the transforms of the step probability density and its time integral. This is a key result for the treatment of space-time coupled CTRW and will be useful for the analytical investigation into the PDF later on.

2.2.2. Transport equation for the PDF in the aged case

For the aged process a slightly more complicated approach is needed. Aging is seen when the walker has started moving before the beginning at observation at $-t_a$ which is illustrated in Fig. 2.4 (taken from [15]). This means that the walker will already be in motion at the beginning of observation, which is set to $t = 0$ and $\mathbf{x} = 0$. He therefore has his first observed change point at some time $t' > 0$, where we denote the probability of this change point being at \mathbf{x}' with $F(\mathbf{x}', t'|t_a)$.

Alternatively the walker can perform a step so long that it stays in continuous motion for the entire duration of observation. In this case no first change point is observed and this event of a long, single step is instead described by $s(\mathbf{x}|t, t_a)$, which is the conditional probability that a walker that has aged for a time t_a performs a step of duration longer than t , such that he is at \mathbf{x} at time t .

The transport equation for the PDF therefore has two terms corresponding to these cases:

$$p(\mathbf{x}|t, t_a) = \int_{\mathbb{R}^d} d^d x' \int_{\mathbb{R}^d} d^d x'' \int_0^t dt' \int_0^{t-t'} dt'' F(\mathbf{x}', t'|t_a) C(\mathbf{x}'', t'') \times r(\mathbf{x} - \mathbf{x}' - \mathbf{x}''|t - t' - t'') + s(\mathbf{x}|t, t_a). \quad (2.28)$$

The second term captures the contribution from the single step case while the double convolution describes a particle having its first change point at t' , then performing a series of completed steps for the duration t'' and then being found at observation time t in a final, incomplete step of duration $t - t' - t''$ or longer, as shown in the upper picture of Fig. 2.4.

A closed expression for $p(\mathbf{k}|s, t_a)$ can be found in the Fourier-Laplace domain by using the convolution properties from Eqs. (2.20) and (2.21) again:

$$p(\mathbf{k}|s, t_a) = F(\mathbf{k}, s|t_a) C(\mathbf{k}, s) r(\mathbf{k}|s) + s(\mathbf{k}|s, t_a). \quad (2.29)$$

2.2.3. Forward waiting time and step rate

Consider again the case where the process has aged for a time t_a : The forward waiting time, $\psi_1(t|t_a)$, gives the probability density that the first change time after the beginning of observation is t when the aging time of the walk is t_a . This is equal to the probability that at some time prior to observation, t' , a step started that lasts until t . This is captured in the integral equation

$$\psi_1(t|t_a) = \int_0^{t_a} k(t') \psi(t_a - t' + t) dt', \quad (2.30)$$

where $k(t)$ is the step rate, i.e. the probability density of starting a new step at time t . ψ_1 and k are the analogs of F and C for random walks without space-time coupling. Indeed one can extract the former by integrating the latter over all of space, which is equivalent to

$$\psi_1(s|t_a) = F(\mathbf{k} = 0, s|t_a), \quad k(s) = C(\mathbf{k} = 0, s), \quad (2.31)$$

in the Fourier-Laplace domain. This close relation makes it useful to know that the forward waiting can be explicitly calculated in the case of a power law time distribution

that lacks the first moment, e.g. the distribution for the generalized Lévy walk (2.2) with $\gamma < 1$. It reads [16]:

$$\psi_1(t|t_a) = \frac{\sin(\pi\gamma)}{\pi} \left(\frac{t_a}{t}\right)^\gamma \frac{1}{t+t_a}. \quad (2.32)$$

Another closely related quantity is the mean number of steps, $\langle n \rangle(t)$, which is related to the step rate via a derivative: $k(t) = \frac{d}{dt} \langle n \rangle(t)$. For the case of a power law distribution with diverging mean, i.e. $\gamma < 1$ the mean number of steps is known to be [16]

$$\langle n \rangle(t) = \frac{1}{\Gamma(1-\gamma)} \frac{t^\gamma}{t_0^\gamma}. \quad (2.33)$$

This implies that the step rate actually decreases with time for $\gamma < 1$. Note that the Lévy walk approaches its asymptotic regime with increasing number of steps. Therefore the result for the mean number of steps suggests that the time it takes for the simulation to reach the asymptotic regime should be proportional to t^γ .

3. Methods

3.1. Method for calculating the MSD

For the calculation of asymptotic behavior of the MSD we concentrate on the one-dimensional case, as this simplifies the calculations. The generalization to higher dimensions is straightforward, because the PDF of the process, Eq. (2.6), is isotropic and the normalization takes care of the angular integration.

The one-dimensional MSD $\langle x^2 \rangle(t)$ is defined via the integral

$$\langle x^2 \rangle(t) = \int_{\mathbb{R}} x^2 \psi(x, t) dx, \quad (3.1)$$

which is closely related to the Fourier-Laplace transform of the PDF for the process, as we can see when we expand it for small k :

$$p(k|s) = \int_{\mathbb{R}} e^{ikx} p(x|s) dx \quad (3.2)$$

$$= \int_{\mathbb{R}} p(x|s) dx + ik \int_{\mathbb{R}} xp(x|s) dx - \frac{k^2}{2} \int_{\mathbb{R}} x^2 p(x|s) dx \quad (3.3)$$

$$= 1 - \frac{k^2}{2} \langle x^2 \rangle(s) + \dots, \quad (3.4)$$

where we used that the PDF is normalized to one and that the first moment of an isotropic process vanishes. This implies

$$\langle x^2 \rangle(s) = - \left[\frac{\partial^2}{\partial k^2} p(k|s) \right]_{k=0}, \quad (3.5)$$

which allows us to calculate the MSD directly without knowledge of the full PDF.

For the ordinary case we can use Eq. (2.26) for the PDF in the Fourier-Laplace domain:

$$p(k|s) = C(k, s) r(k|s). \quad (3.6)$$

We now expand C and r similarly to what we did for the PDF, resulting in

$$r(k|s) = r_0(s) - \frac{1}{2}k^2 r_2(s) + o(k^2), \quad (3.7)$$

$$C(k, s) = C_0(s) - \frac{1}{2}k^2 C_2(s) + o(k^2). \quad (3.8)$$

Here the first moments vanish again and we introduced the following notation for the marginal moments:

$$r_0(s) = r(k=0|s), \quad r_2(s) = \left[\frac{\partial^2}{\partial k^2} r(k|s) \right]_{k=0}, \quad (3.9)$$

$$C_0(s) = C(k=0|s), \quad C_2(s) = \left[\frac{\partial^2}{\partial k^2} C(k|s) \right]_{k=0}. \quad (3.10)$$

Inserting these expansions into Eq. (3.6) we find for the PDF

$$p(k|s) = C_0(s)r_0(s) - \frac{k^2}{2} [C_0(s)r_2(s) + C_2(s)r_0(s)] + o(k^2), \quad (3.11)$$

from which it follows by Eq. (3.5) that in the ordinary case the MSD is given by

$$\langle x^2 \rangle(s) = C_0(s)r_2(s) + C_2(s)r_0(s). \quad (3.12)$$

For the aged case we start from the result found in Eq. (2.29),

$$p(k|s, t_a) = F(k, s|t_a)C(k, s)r(k|s) + s(k|s, t_a), \quad (3.13)$$

and use a similar expansions for the transforms of the single step density and the first step density:

$$s(k|s, t_a) = s_0(s, t_a) - \frac{1}{2}k^2 s_2(s, t_a) + o(k^2), \quad (3.14)$$

$$F(k, s|t_a) = F_0(s|t_a) - \frac{1}{2}k^2 F_2(s|t_a) + o(k^2). \quad (3.15)$$

Thus we find for the PDF

$$p(k|s) = F_0(s|t_a)C_0(s)r_0(s) - \frac{k^2}{2} [F_0(s|t_a)C_0(s)r_2(s) + F_0(s|t_a)C_2(s)r_0(s) + F_2(s|t_a)C_0(s)r_0(s) + s_2(s, t_a)] + o(k^2). \quad (3.16)$$

Again using Eq. (3.5) we obtain for the MSD in the aged case:

$$\begin{aligned} \langle x^2 \rangle(s) = & F_0(s|t_a)C_0(s)r_2(s) + F_0(s|t_a)C_2(s)r_0(s) \\ & + F_2(s|t_a)C_0(s)r_0(s) + s_2(s, t_a). \end{aligned} \quad (3.17)$$

To extract the asymptotic results from Eqs. (3.12) and (3.17) we need to look at the $t \rightarrow \infty$ limit, which corresponds to the $s \rightarrow 0$ limit in the Laplace domain.

The general strategy is therefore to find expressions for the quantities $C_0, F_0, r_0, C_2, F_2, r_2$ in the Laplace domain to leading order in s . They are then inserted into the respective equations for the MSD, which is then transformed back into the time domain. s_2 can be calculated directly in the time domain, as it is not part of a product in the expression for the aged MSD.

The key tool for moving between the Laplace and the time domain is the Tauberian theorem. It states that the Laplace transform of a function $f(t)$ following a power law for large t through the formula [16]

$$f(t) \simeq t^{\rho-1} L(t) \leftrightarrow f(s) \simeq \Gamma(\rho) s^{-\rho} L\left(\frac{1}{s}\right), \quad (3.18)$$

if $\rho \geq 0$ and $L(t)$ is slowly varying, i.e. when

$$\lim_{t \rightarrow \infty} \frac{L(C t)}{L(t)} = 1. \quad (3.19)$$

For general ρ the slightly more complicated formula

$$f(s) \simeq \sum_{k=0}^{k_{\max}} \frac{(-1)^k}{k!} I_k^f s^k + L\Gamma(\rho) s^{-\rho}, \quad (3.20)$$

has to be used, which is derived in Sec. A. Here k_{\max} is the whole part of $-\rho$, and I_k^f is the moment integral

$$I_k^f = \int_0^\infty t^k f(t) dt. \quad (3.21)$$

3.2. Method for calculating the PDF

So far no analytic solution for the PDF of the original Lévy walk is known for general values of γ and ν , which makes finding it for the generalized model a difficult task. However there is a remarkable result by Magdziarz, who found closed expressions for the PDF in any dimension for the special case $\nu = 1$ (i.e. the velocity model) [21,22]. It is therefore tempting to see if his method might be generalized and applied to our case. Unfortunately this turned out to be impossible, as his technique for performing the inverse transform relied heavily on the scaling of the transformed PDF, $p(\mathbf{k}|s) \propto f\left(\frac{k}{s}\right)$, which is not preserved when ν deviates from 1. In this case the function scales as $p(\mathbf{k}|s) \propto f\left(\frac{k}{s^\nu}\right)$ which makes the method unworkable for arbitrary ν .

Instead an asymptotic approach is taken, where the starting point for the calculation

is the general expression for the transformed PDF found in Eq. (2.27):

$$p(\mathbf{k}|s) = \frac{r(\mathbf{k}|s)}{1 - \psi(\mathbf{k}, s)}. \quad (3.22)$$

Here an expansion is again performed for the one dimensional PDF, analogously to the calculation of the MSD.

For the inverse Laplace transform analytical results are supplemented with the use of numerical inverse transforms. These can be performed efficiently through the use of the algorithm proposed by Talbot [23], which has been slightly improved and implemented in Mathematica in [24].

3.3. Numerical simulation of the model

Numerical simulations supplement and support analytical computations by giving insight into the qualitative structure of the process, sharpening the understanding of the model and giving a method of testing the results. Furthermore numerical methods allow the investigation of regimes where no analytical solution can be found.

The simulation implemented for this thesis creates an ensemble of Lévy walkers, each of which performing steps whose length and direction is determined by a pseudorandom number generator. Information about the process is then extracted by averaging over the ensemble.

The two main quantities that we are interested in for this thesis are the MSD and the PDF of the generalized Lévy walk: The former can be found by computing the position of the walkers at preset measurement times and taking the ensemble averages. For the latter the distance from the origin is split into intervals with bins that track the number of particles in that region. The PDF can then be approximated by plotting the bins in a histogram. This was implemented in one dimension similarly to the analytical computation, as this captures most of the behavior in an isotropic walk.

The computation time of the simulation depends mainly on the number of steps that have to be computed and the size of the ensemble. As we have seen in the theory section the average number of steps scales with t^γ . This means that the duration of the walk, t , is the main parameter for influencing the number of steps. In particular we can choose lower walk durations for simulations with high γ values to keep the computation time reasonable.

The second limiting factor for performance is the ensemble size, which is of special importance for processes with power law distributions such as Lévy walks, because these processes are dominated by rare events which are only captured with sufficiently large ensembles.

To address this issue I use the independence of the different walkers to parallelize the computation and perform it on the available graphics cards (GPUs) using NVIDIA's

C++ extension CUDA. The university computers are equipped with Quadro K4000 GPUs, that have 768 cores each. This is a far greater than the number of cores available on a typical processor (CPU), which is usually less than ten, and thus allows for far greater parallelization, resulting in a theoretical speedup of over 70.

In praxis this is not quite reached, because of the GPU cores being slower individually, the latency in the data transfer between CPU and GPU as well as the smaller memory on the GPU (3GB). However by saving only the sum of squared displacements at selected measurement times and reducing communication between GPU and CPU to a minimum it was possible to simulate large ensembles of 10^9 walkers in a few hours.

Another aspect that should be addressed is the generation of pseudorandom numbers for the creation of the steps for the simulation. As these numbers are not truly random, i.e. not completely uncorrelated, they can, depending on the quality of the number generator, leave statistical artifacts that falsify the simulation results. To minimize this risk I use the cuRAND library, which implements a version of the powerful Xorshift algorithm [25]. The documentation guarantees a period greater than 2^{190} for each independently seeded sequence of random numbers (i.e. each simulation), and each thread has an offset of 2^{67} in this sequence. In the simulation no more than 10^9 walkers are used, so we have a total offset of $10^9 \cdot 2^{67} \simeq 2^{97} \ll 2^{190}$. In each individual thread the walker performs typically fewer than $10^7 \simeq 2^{23}$ steps, which is much smaller than the offset of 2^{67} . The risk that statistical artifacts influence the results is therefore very small.

4. Analytical Calculations

4.1. MSD in the ordinary case

The calculation of the MSD, both in the ordinary and in the aged case originally appeared in [15] and are presented here again:

Calculation of $\psi_0(s)$

All properties of the ordinary walk are derived from the waiting time density $\psi(t)$. The joint probability density of the displacement in a step and the duration of a step is given in the one dimensional case by

$$\psi(x, t) = \frac{1}{2} \delta(|x| - ct^\nu) \psi(t), \quad (4.1)$$

so that the Fourier transform of this function in the x variable reads

$$\psi(k, t) = \psi(t) - \frac{k^2}{2} c^2 t^{2\nu} \psi(t) + o(k^2). \quad (4.2)$$

Then the Laplace transform in t should be performed. We are only interested in the asymptotic behavior, which can be found using the Tauberian theorem (3.20). The forms of the Laplace transform differ for different values of γ and ν . As explained above we are interested only in the lowest order terms of s -dependence.

$$\gamma < 1$$

For $0 < \gamma < 1$ the function $\psi_0(s) = \psi(s)$ belongs to an integrable class, and its Laplace representation reads

$$\psi_0(s) \simeq 1 + \gamma \Gamma(-\gamma) t_0^\gamma s^\gamma = 1 - \Gamma(1 - \gamma) t_0^\gamma s^\gamma. \quad (4.3)$$

Keeping t_0 in all calculations and not putting it to unity is reasonable to be able to check the dimension of the ensuing results, especially in the aged case.

$$\gamma > 1$$

The Laplace transform of $\psi(t)$ now has an additional term, due to its first moment being finite:

$$\psi_0(s) \simeq 1 - \tau s - \Gamma(1 - \gamma)t_0^\gamma s^\gamma. \quad (4.4)$$

Here τ is defined as

$$\tau = \frac{\gamma}{t_0} \int_0^\infty \frac{t dt}{(1 + t/t_0)^{\gamma+1}} = \frac{t_0}{\gamma - 1}. \quad (4.5)$$

Calculation of $\psi_2(s)$

The marginal second moment of the step distribution is given by

$$\psi_2(t) = \int_{-\infty}^\infty x^2 \psi(x, t) dx = c^2 t^{2\nu} \psi(t). \quad (4.6)$$

The expressions for $\psi_2(s)$ depend on whether $2\nu < \gamma$ or $2\nu > \gamma$:

$$2\nu < \gamma$$

In this first case the function $\psi_2(t)$ is integrable, $\int_0^\infty \psi_2(t) dt < \infty$, and the expansion of its Laplace transform starts from a constant:

$$\psi_2(s) \simeq \gamma c^2 t_0^{2\nu} \int_0^\infty \frac{x^{2\nu}}{(1+x)^{\gamma+1}} dx + \gamma \Gamma(2\nu - \gamma) c^2 t_0^\gamma s^{\gamma-2\nu}, \quad (4.7)$$

where the integral is given by a dimensionless constant:

$$\int_0^\infty \frac{x^{2\nu}}{(1+x)^{\gamma+1}} dx = B(2\nu + 1, \gamma - 2\nu), \quad (4.8)$$

with $B(a, b)$ being the Beta-function, which is defined as:

$$B(a, b) = \int_0^1 x^{a-1} (1-x)^{b-1} dx = \frac{\Gamma(a)\Gamma(b)}{\Gamma(a+b)}. \quad (4.9)$$

With this $\psi_2(s)$ takes the form

$$\psi_2(s) \simeq \gamma c^2 t_0^{2\nu} B(2\nu + 1, \gamma - 2\nu) + \gamma \Gamma(2\nu - \gamma) c^2 t_0^\gamma s^{\gamma-2\nu}. \quad (4.10)$$

$$2\nu > \gamma$$

In the second case $\psi_2(t)$ is non-integrable, the integral $\int_0^\infty \psi_2(t)dt$ diverges, and the asymptotics of its Laplace transform read

$$\psi_2(s) \simeq \gamma \Gamma(2\nu - \gamma) c^2 t_0^\gamma s^{\gamma-2\nu}. \quad (4.11)$$

Calculation of $C_0(s)$ and $C_2(s)$

For complete steps our generalization does not differ from the original Lévy walk and we can use the general result for $C(x, t)$ in the Fourier-Laplace domain Eq. (2.23):

$$C(k, s) = \frac{1}{1 - \psi(k, s)}. \quad (4.12)$$

Expanding $C(k, s)$ for s small and in the limit $k \rightarrow 0$ we find

$$\begin{aligned} C(k, s) &\simeq \frac{1}{1 - \psi(s) + (k^2/2)\psi_2(s) + o(k^2)} \\ &\simeq \frac{1}{1 - \psi(s)} - \frac{k^2}{2} \frac{\psi_2(s)}{[1 - \psi(s)]^2} + o(k^2). \end{aligned} \quad (4.13)$$

Therefore

$$C_0(s) = \frac{1}{1 - \psi(s)}, \quad (4.14)$$

$$C_2(s) = \frac{\psi_2(s)}{[1 - \psi(s)]^2}, \quad (4.15)$$

into which we now have to insert our results for ψ_0 and ψ_2 :

$$\gamma < 1 \text{ and } 2\nu < \gamma$$

Here we find by using equations (4.3) and (4.10) :

$$C_0(s) \simeq \frac{1}{\Gamma(1 - \gamma)} t_0^{-\gamma} s^{-\gamma}, \quad (4.16)$$

$$C_2(s) \simeq \gamma \frac{B(2\nu + 1, \gamma - 2\nu)}{\Gamma^2(1 - \gamma)} c^2 t_0^{2\nu-2\gamma} s^{-2\gamma}. \quad (4.17)$$

$\gamma < 1$ **and** $2\nu > \gamma$:

In this case we obtain for C_2 :

$$C_2(s) \simeq \gamma \frac{\Gamma(2\nu - \gamma)}{\Gamma^2(1 - \gamma)} c^2 t_0^{-\gamma} s^{-2\nu - \gamma}, \quad (4.18)$$

while C_0 is the same as in Eq.(4.16) as long as $\gamma < 1$.

$\gamma > 1$ **and** $2\nu < \gamma$

Now the first moment of $\psi(t)$ is finite, therefore

$$C_0(s) \simeq \frac{1}{\tau s} \quad (4.19)$$

$$C_2(s) \simeq \gamma B(2\nu + 1, \gamma - 2\nu) c^2 \frac{t_0^{2\nu}}{\tau^2} s^{-2} \quad (4.20)$$

$\gamma > 1$ **and** $2\nu > \gamma$:

Again $C_0(s)$ doesn't change, and for C_2 we obtain

$$C_2 \simeq \gamma \Gamma(2\nu - \gamma) c^2 \frac{t_0^\gamma}{\tau^2} s^{\gamma - 2\nu - 2}. \quad (4.21)$$

Calculation of $r_0(s)$ and $r_2(s)$

The function $r(x|t)$ gives the distribution of the corresponding displacements conditioned on the fact that the total duration of a step is longer than t . In Eq. (2.24) we found the expression

$$r(x|t) = \int_t^\infty \frac{1}{2} \delta(|x| - ct^\eta t'^{\nu - \eta}) \psi(t') dt'. \quad (4.22)$$

This is correctly normalized to the overall probability to stay within a single step for a time longer than t

$$\int_{-\infty}^\infty r(x|t) dx = \int_t^\infty \psi(t') dt'. \quad (4.23)$$

Expanding the Fourier transform of $r(x, t)$ for small k ,

$$\begin{aligned} r(k|t) &= \int_{-\infty}^{\infty} dx e^{ikx} \int_t^{\infty} \frac{1}{2} \delta(|x| - ct^\eta t'^{\nu-\eta}) \psi(t') dt' \\ &= r_0(t) - \frac{k^2}{2} r_2(t) + o(k^2), \end{aligned} \quad (4.24)$$

we find the marginal moments

$$r_0(t) = \frac{1}{(1 + t/t_0)^\gamma} \quad (4.25)$$

$$r_2(t) = \gamma c^2 \frac{1}{t_0} t^{2\eta} \int_t^{\infty} \frac{t'^{2(\nu-\eta)}}{(1 + t'/t_0)^{\gamma+1}} dt', \quad (4.26)$$

whose Laplace transforms depend on the relationship between γ , ν and η :

$$\gamma < 1$$

In this case r_0 is non-integrable and we find

$$r_0(s) \simeq \Gamma(1 - \gamma) t_0^\gamma s^{\gamma-1}. \quad (4.27)$$

For r_2 we can use the asymptotic form of $\psi(t)$, since we are interested in large t :

$$r_2(t) \simeq \gamma c^2 t_0^\gamma t^{2\eta} \int_t^{\infty} \tau^{2(\nu-\eta)-1-\gamma} d\tau, \quad (4.28)$$

which is only finite for $\gamma > 2(\nu - \eta)$ and diverges otherwise, meaning that no MSD exists. In the rest of the paper we will concentrate on the case when the MSD is finite, where we find

$$r_2(t) \simeq \gamma \frac{1}{\gamma - 2(\nu - \eta)} c^2 t_0^\gamma t^{2\nu-\gamma}. \quad (4.29)$$

Since this expression is always in the non-integrable class we obtain the following result by using the Tauberian theorem (3.18):

$$r_2(s) \simeq \gamma \frac{\Gamma(2\nu + 1 - \gamma)}{\gamma - 2(\nu - \eta)} c^2 t_0^\gamma s^{\gamma-2\nu-1}. \quad (4.30)$$

$$\gamma > 1 \text{ and } 2\nu > \gamma - 1$$

For $\gamma > 1$ $r_0(t)$ becomes integrable, therefore its Laplace transform reads

$$r_0 \simeq \tau + \Gamma(1 - \gamma) t_0^\gamma s^{\gamma-1}. \quad (4.31)$$

The function $r_2(t)$ is still non-integrable and therefore identical to the previous case.

$\gamma > 1$ **and** $2\nu < \gamma - 1$

In this case r_0 does not change but $r_2(s)$ is now integrable and therefore its transform behaves as

$$r_2(s) \simeq I_0^{r_2} - \gamma \frac{\Gamma(2\nu + 1 - \gamma)}{2(\nu - \eta) - \gamma} c^2 t_0^\gamma s^{\gamma-2\nu-1}. \quad (4.32)$$

We evaluate the definite integral $I_0^{r_2}$ by manipulating the area of integration:

$$\begin{aligned} I_0^{r_2} &= c^2 \int_0^\infty dt t^{2\eta} \int_t^\infty dt' \psi(t') (t')^{2(\nu-\eta)} \\ &= c^2 \frac{1}{2\eta + 1} \int_0^\infty \psi(t') t'^{2\nu+1} dt' \\ &= \gamma \frac{1}{2\eta + 1} \int_0^\infty \frac{x^{2\nu+1} dx}{(1+x)^{\gamma+1}} c^2 t_0^{2\nu+1} \\ &= \gamma \frac{B(2\nu + 2, \gamma - 2\nu - 1)}{2\eta + 1} c^2 t_0^{2\nu+1}, \end{aligned} \quad (4.33)$$

$$= \gamma \frac{B(2\nu + 2, \gamma - 2\nu - 1)}{2\eta + 1} c^2 t_0^{2\nu+1}, \quad (4.34)$$

meaning the r_2 is constant in the leading order. Therefore we find for $\gamma > 1$ and $2\nu < \gamma - 1$

$$r_2 \simeq \gamma \frac{B(2\nu + 2, \gamma - 2\nu - 1)}{2\eta + 1} c^2 t_0^{2\nu+1} - \gamma \frac{\Gamma(2\nu + 1 - \gamma)}{2(\nu - \eta) - \gamma} c^2 t_0^\gamma s^{\gamma-2\nu-1}. \quad (4.35)$$

The results so far are summarized in Table 4.1.

$\gamma < 1$	$C_0(s) \simeq \frac{1}{\Gamma(1-\gamma)} t_0^{-\gamma} s^{-\gamma}$	$C_2(s) \simeq \begin{cases} \gamma \frac{B(2\nu+1, \gamma-2\nu)}{\Gamma^2(1-\gamma)} c^2 t_0^{2\nu-2\gamma} s^{-2\gamma} & \text{for } 2\nu < \gamma \\ \gamma \frac{\Gamma(2\nu-\gamma)}{\Gamma^2(1-\gamma)} c^2 t_0^{-\gamma} s^{-2\nu-\gamma} & \text{for } 2\nu > \gamma \end{cases}$
$\gamma < 1$	$r_0(s) \simeq \Gamma(1-\gamma) t_0^\gamma s^{\gamma-1}$	$r_2(s) \simeq \gamma \frac{\Gamma(2\nu+1-\gamma)}{\gamma-2(\nu-\eta)} c^2 t_0^\gamma s^{\gamma-1-2\nu}$
$\gamma > 1$	$C_0(s) \simeq \frac{1}{\tau s}$	$C_2(s) \simeq \begin{cases} \gamma B(2\nu + 1, \gamma - 2\nu) c^2 \frac{t_0^{2\nu}}{\tau^2} s^{-2} & \text{for } 2\nu < \gamma \\ \gamma \Gamma(2\nu - \gamma) c^2 \frac{t_0^\gamma}{\tau^2} s^{\gamma-2\nu-2} & \text{for } 2\nu > \gamma \end{cases}$
$\gamma > 1$	$r_0(s) \simeq \tau$	$r_2(s) \simeq \begin{cases} \gamma \frac{B(2\nu+2, \gamma-2\nu-1)}{2\eta+1} c^2 t_0^{2\nu+1} & \text{for } 2\nu < \gamma - 1 \\ \gamma \frac{\Gamma(2\nu+1-\gamma)}{\gamma-2(\nu-\eta)} c^2 t_0^\gamma s^{\gamma-2\nu-1} & \text{for } 2\nu > \gamma - 1 \end{cases}$

Table 4.1.: Leading terms of the marginal moments of C and r in the Laplace domain for different parameter ranges.

Mean squared displacement

With these results we can now compute the MSD via the formula

$$\langle x^2(s) \rangle = C_0(s)r_2(s) + C_2(s)r_0(s). \quad (4.36)$$

$\gamma < 1$ **and** $2\nu < \gamma$:

In the case $2\nu < \gamma$ we have

$$\begin{aligned} \langle x^2(s) \rangle \simeq \gamma & \left[\frac{\Gamma(2\nu + 1 - \gamma)}{\Gamma(1 - \gamma)(\gamma - 2(\nu - \eta))} c^2 s^{-2\nu-1} \right. \\ & \left. + \frac{B(2\nu + 1, \gamma - 2\nu)}{\Gamma(1 - \gamma)} c^2 t_0^{2\nu-\gamma} s^{-\gamma-1} \right], \end{aligned} \quad (4.37)$$

which translates to

$$\begin{aligned} \langle x^2(t) \rangle \simeq \gamma & \left[\frac{\Gamma(2\nu + 1 - \gamma)}{\Gamma(1 - \gamma)(\gamma - 2(\nu - \eta))\Gamma(2\nu + 1)} c^2 t^{2\nu} \right. \\ & \left. + \frac{B(2\nu + 1, \gamma - 2\nu)}{\Gamma(1 - \gamma)\Gamma(1 + \gamma)} c^2 t_0^{2\nu-\gamma} t^\gamma \right]. \end{aligned} \quad (4.38)$$

This is dominated by the second term since $2\nu < \gamma$, leading to $\langle x^2(t) \rangle \propto t^\gamma$ in this case.

$\gamma < 1$ **and** $2\nu > \gamma$

In this parameter regime we obtain

$$\begin{aligned} \langle x^2(s) \rangle & \simeq \gamma c^2 s^{-2\nu-1} \left[\frac{\Gamma(2\nu + 1 - \gamma)}{\Gamma(1 - \gamma)(\gamma - 2(\nu - \eta))} + \frac{\Gamma(2\nu - \gamma)}{\Gamma(1 - \gamma)} \right] \\ & = \gamma \frac{\Gamma(2\nu - \gamma)}{\Gamma(1 - \gamma)} \frac{2\eta}{\gamma - 2(\nu - \eta)} c^2 s^{-2\nu-1}, \end{aligned} \quad (4.39)$$

therefore we find in the time domain

$$\langle x^2(t) \rangle \simeq \gamma \frac{\Gamma(2\nu - \gamma)}{\Gamma(2\nu + 1)\Gamma(1 - \gamma)} \frac{2\eta}{2(\nu - \eta) - \gamma} c^2 t^{2\nu}. \quad (4.40)$$

$\gamma > 1$ **and** $2\nu < \gamma - 1$

In this case the MSD reads

$$\begin{aligned}\langle x^2(s) \rangle &= C_0(s)r_2(s) + C_2(s)r_0(s) \\ &\simeq \gamma \frac{B(2\nu + 2, \gamma - 2\nu - 1)}{2\eta + 1} c^2 \frac{t_0^{2\nu+1}}{\tau} \frac{1}{s} + \gamma B(2\nu + 1, \gamma - 2\nu) c^2 \frac{t_0^{2\nu}}{\tau} s^{-2},\end{aligned}$$

which is dominated by the second term. Therefore we find in the time domain to leading order:

$$\langle x^2(t) \rangle \simeq \gamma B(2\nu + 1, \gamma - 2\nu) c^2 \frac{t_0^{2\nu}}{\tau} t. \quad (4.41)$$

$\gamma > 1$ **and** $\gamma - 1 < 2\nu < \gamma$

Compared to the previous case only r_2 changes, therefore

$$\langle x^2(s) \rangle \simeq \gamma \frac{\Gamma(2\nu + 1 - \gamma)}{\gamma - 2(\nu - \eta)} c^2 \frac{t_0^\gamma}{\tau} s^{\gamma-2-2\nu} + \gamma B(2\nu + 1, \gamma - 2\nu) c^2 \frac{t_0^{2\nu}}{\tau} s^{-2}. \quad (4.42)$$

Since $\gamma - 2\nu > 0$ the term quadratic in s is again dominant, and the asymptotic behavior in the time domain is identical to the previous case:

$$\langle x^2(t) \rangle \simeq \gamma B(2\nu + 1, \gamma - 2\nu) c^2 \frac{t_0^{2\nu}}{\tau} t. \quad (4.43)$$

$\gamma > 1$ **and** $2\nu > \gamma$

Now C_2 is different, giving us

$$\langle x^2(s) \rangle \simeq \gamma \frac{\Gamma(2\nu + 1 - \gamma)}{\gamma - 2(\nu - \eta)} c^2 \frac{t_0^\gamma}{\tau} s^{\gamma-2\nu-2} + \gamma \Gamma(2\nu - \gamma) c^2 \frac{t_0^\gamma}{\tau} s^{\gamma-2\nu-2}. \quad (4.44)$$

This leads to the time dependence

$$\langle x^2(t) \rangle \simeq \gamma \frac{2\eta}{\gamma - 2(\nu - \eta)} \frac{\Gamma(2\nu - \gamma)}{\Gamma(2\nu + 2 - \gamma)} c^2 \frac{t_0^\gamma}{\tau} t^{2\nu+1-\gamma}. \quad (4.45)$$

The results for the ordinary walk under the assumption that the convergence condition

$\gamma > 2(\nu - \eta)$ is satisfied can be summarized as follows:

$$\langle x^2(t) \rangle \propto \begin{cases} t^\gamma & \text{for } \gamma < 1, 2\nu < \gamma \\ t^{2\nu} & \text{for } \gamma < 1, 2\nu > \gamma \\ t & \text{for } \gamma > 1, 2\nu < \gamma \\ t^{2\nu+1-\gamma} & \text{for } \gamma > 1, 2\nu > \gamma. \end{cases} \quad (4.46)$$

Thus, in the whole domain of γ there are four regimes with crossovers at $\gamma = 1$ and at $2\nu = \gamma$:

- For $2\nu < \gamma$ one has $\langle x^2(t) \rangle \propto t^\gamma$ for $\gamma < 1$ crossing over to a faster growth $\langle x^2(t) \rangle \propto t$ for $\gamma > 1$
- For $2\nu > \gamma$ one has universally $\langle x^2(t) \rangle \propto t^{2\nu}$ for $\gamma < 1$ crossing over to a slower growth $\langle x^2(t) \rangle \propto t^{2\nu+1-\gamma}$ for $\gamma > 1$.

4.2. MSD in the aged case: general expressions

We now consider the functions F and s which are specific to aged walks. The general expression for F reads:

$$F(x, t|t_a) = \int_0^{t_a} dt' \psi(t_a + t - t') k(t') \times \frac{1}{2} \delta \left\{ |x| - c[(t_a + t - t')^\nu - (t_a + t - t')^{\nu-\eta}(t_a - t')^\eta] \right\}, \quad (4.47)$$

where $k(t) = C_0(t)$ is the time-dependent rate of steps. Note that the argument of the δ -function is shifted, due to the fact that the distance from the origin x is set to zero at the start of the measurement. The marginal density of $F(x, t|t_a)$ is

$$F_0(t|t_a) = \int F(x, t|t_a) dx = \int_0^{t_a} \psi(t_a + t - t') k(t') dt' = \psi_1(t|t_a), \quad (4.48)$$

where $\psi_1(t|t_a)$ is the forward waiting time PDF known from the theory of CTRW as discussed in Sec. (2.2.3). The marginal second moment of F reads:

$$F_2(t|t_a) = \int_0^{t_a} dt' c^2 \psi(t_a + t - t') k(t') \times [(t_a + t - t')^\nu - (t_a + t - t')^{\nu-\eta}(t_a - t')^\eta]^2. \quad (4.49)$$

Additionally we have to consider the term $s(x|t, t_a)$, which describes the case that both the aging time and the observation time belong to the same step:

$$s(x|t, t_a) = \int_0^{t_a} dt' k(t') \int_{t_a+t-t'}^{\infty} dt'' \psi(t'') \quad (4.50)$$

$$\times \frac{1}{2} \delta \left\{ |x| - c[(t'')^{\nu-\eta}(t_a+t-t')^\eta - (t'')^{\nu-\eta}(t_a-t')^\eta] \right\},$$

where the inner integral gives the probability that no change point took place during the time interval between t' and $t_a + t$. The zeroth order of this function,

$$s_0(t, t_a) = \int_0^{t_a} \Psi(t_a + t - t') k(t') dt', \quad (4.51)$$

where $\Psi(t) = \int_t^\infty \psi(t') dt'$ is the survival probability, is not necessary for what follows, and will not be calculated.

The second moment is given by

$$s_2(t, t_a) = c^2 \int_0^{t_a} k(t') \int_{t_a+t-t'}^{\infty} \psi(t'') \quad (4.52)$$

$$\times [(t'')^{\nu-\eta}(t_a+t-t')^\eta - (t'')^{\nu-\eta}(t_a-t')^\eta]^2 dt'' dt'.$$

We note that the form of the integrals involved in F_2 and s_2 is similar. In the following calculation we differentiate between two time regimes: The case of short aging times $t \gg t_a \gg t_0$ and the case of long aging times $t_a \gg t \gg t_0$, which will be discussed separately in the two following sections.

4.3. MSD in the aged case: short aging times

Calculation of F_0 and F_2

First consider the limit $t \gg t_a$: We are interested in the Laplace transforms of the marginal moments of F_0 and F_2 . Since both of them depend on $k(t) = C_0(t)$ whose form we found to be dependent on whether $\gamma < 1$ or $\gamma > 1$, so we have to distinguish between these cases:

$$\gamma < 1$$

The function $F_0(t|t_a)$ is equal to the forward waiting time PDF $\psi_1(t|t_a)$. For $\gamma < 1$ we can use the result from Eq. (2.32)

$$F_0(t|t_a) = \psi_1(t|t_a) = \frac{\sin \pi \gamma}{\pi} \left(\frac{t_a}{t} \right)^\gamma \frac{1}{t + t_a}. \quad (4.53)$$

The expression is normalized to unity, and therefore in the Laplace domain the leading term in F_0 will be 1.

For $t \gg t_a$ the expression in the square brackets in Eq.(4.49) can be approximated by $t^{2\nu}$ (since $\nu > 0$) and for F_2 we find in this limit

$$F_2(t|t_a) \simeq c^2 t^{2\nu} \int_0^{t_a} \psi(t_a + t - t') k(t') dt'. \quad (4.54)$$

The integral can again be expressed through the forward waiting time $\psi_1(t|t_a)$. We take the asymptotics of ψ_1 for t large, so that

$$F_2(t|t_a) \simeq \frac{\sin \pi \gamma}{\pi} c^2 t_a^\gamma t^{2\nu-\gamma-1}. \quad (4.55)$$

Here again two situations arise depending on the integrability:

$\gamma < 1$ **and** $2\nu > \gamma$

In this case F_2 is non-integrable, so that in the Laplace domain

$$F_2(s|t_a) \simeq \Gamma(2\nu - \gamma) \frac{\sin \pi \gamma}{\pi} c^2 t_a^\gamma s^{\gamma-2\nu}. \quad (4.56)$$

$\gamma < 1$ **and** $2\nu < \gamma$

Now F_2 is integrable, and the lowest order in its Laplace transform tends to a constant:

$$F_2(s|t_a) \simeq \frac{\sin \pi \gamma}{\pi} c^2 t_a^\gamma \int_0^\infty \frac{t^{2\nu-\gamma}}{t + t_a} dt. \quad (4.57)$$

The corresponding integral is given by

$$\int_0^\infty \frac{t^{2\nu-\gamma}}{t + t_a} dt = \frac{\pi}{\sin(\pi(2\nu + 1 - \gamma))} t_a^{2\nu-\gamma}, \quad (4.58)$$

see Eq.(2.2.5.25) of Ref. [26], so that

$$F_2(s|t_a) \simeq \frac{\sin \pi \gamma}{\sin(\pi(2\nu + 1 - \gamma))} c^2 t_a^{2\nu}. \quad (4.59)$$

$\gamma > 1$

Now we consider the case $\gamma > 1$. From the previous section we know that $C_0(s) = \frac{1}{\tau s}$, therefore

$$k(t) = C_0(t) = \frac{1}{\tau}. \quad (4.60)$$

With this we can rewrite F_0 as

$$F_0(t|t_a) = \frac{1}{\tau} \int_0^{t_a} \psi(t+y) dy. \quad (4.61)$$

For $t \rightarrow \infty$ the integral decays as $t^{-\gamma-1}$ and therefore is of integrable type. To find its lowest order (constant) term of the Laplace transform we note that

$$F_0(s|t_a) \simeq \frac{1}{\tau} \int_0^\infty dt \int_0^{t_a} \psi(t+y) dy \quad (4.62)$$

$$= \frac{1}{\tau} \int_0^{t_a} dy \int_0^\infty dt \psi(t+y) \quad (4.63)$$

$$= \frac{1}{\tau} \int_0^{t_a} dy \int_y^\infty dt \psi(t) \quad (4.64)$$

$$= \frac{1}{\tau} \int_0^{t_a} \Psi(y) dy, \quad (4.65)$$

where $\Psi(t) = \int_t^\infty dt' \psi(t')$ is the so-called survival probability which is normalized to $\int_0^\infty \Psi(t') dt' = \tau$. Since $t_a \gg t_0$ the whole integral therefore tends to τ .

The term F_2 for $t \gg t_a$ can again be evaluated by approximating the expression in square brackets in Eq.(4.49) by t^ν :

$$F_2(t|t_a) \simeq c^2 \frac{1}{\tau} t^{2\nu} \int_0^{t_a} \psi(t+y) dy \quad (4.66)$$

$$= c^2 \frac{t_0^\gamma}{\tau} [(t+t_0)^{-\gamma} - (t+t_a+t_0)^{-\gamma}] t^{2\nu}. \quad (4.67)$$

Since the power law asymptotics of the expression in square brackets are $t^{-\gamma-1}$ the whole expression

$$F_2(t|t_a) \simeq \gamma c^2 \frac{t_0^\gamma}{\tau} t_a t^{2\nu-\gamma-1} \quad (4.68)$$

is of the non-integrable type for $2\nu > \gamma$ and of integrable type for $2\nu < \gamma$.

$\gamma > 1$ **and** $2\nu > \gamma$

In this first case $F_2(t|t_a)$ is non-integrable, therefore the Laplace transform is

$$F_2(s|t_a) \simeq \gamma \Gamma(2\nu - \gamma) c^2 \frac{t_0^\gamma}{\tau} t_a s^{\gamma-2\nu}. \quad (4.69)$$

$\gamma > 1$ **and** $2\nu < \gamma$

In the second case the Laplace transform of the expression tends to a constant. To evaluate this we put down

$$F_2 \simeq \gamma c^2 \frac{t_0^\gamma}{\tau} \int_0^\infty dt t^{2\nu} \int_0^{t_a} \frac{1}{(t + t_0 + y)^{\gamma+1}} dy, \quad (4.70)$$

and interchange the sequence of integrations:

$$\begin{aligned} F_2 &= \gamma c^2 \frac{t_0^\gamma}{\tau} \int_0^{t_a} dy \int_0^\infty \frac{t^{2\nu}}{(t + t_0 + y)^{\gamma+1}} dt \\ &= \gamma B(2\nu + 1, \gamma - 2\nu) c^2 \frac{t_0^\gamma}{\tau} \int_0^{t_a} (t_0 + y)^{2\nu-\gamma} dy \\ &= \gamma \frac{B(2\nu + 1, \gamma - 2\nu)}{2\nu + 1 - \gamma} c^2 \frac{t_0^\gamma}{\tau} [(t_0 + t_a)^{2\nu+1-\gamma} - t_0^{2\nu+1-\gamma}]. \end{aligned}$$

(in the transition to the second line the Eq.(2.2.5.24) of Ref. [26] is used). The corresponding expression is dominated by the first or by the second term in the square brackets, depending on whether $2\nu > \gamma - 1$ or $2\nu < \gamma - 1$.

We summarize our results for $\gamma > 1$ in the following formula:

$$F_2 = \begin{cases} \gamma \frac{B(2\nu+1, \gamma-2\nu)}{\gamma-1-2\nu} c^2 \frac{t_0^{2\nu+1}}{\tau} & \text{for } 2\nu < \gamma - 1 \\ \gamma \frac{B(2\nu+1, \gamma-2\nu)}{2\nu-\gamma+1} c^2 \frac{t_0^\gamma}{\tau} t_a^{2\nu+1-\gamma} & \text{for } \gamma - 1 < 2\nu < \gamma \\ \gamma \Gamma(2\nu - \gamma) c^2 \frac{t_0^\gamma}{\tau} t_a s^{\gamma-2\nu} & \text{for } 2\nu > \gamma \end{cases} \quad (4.71)$$

Calculation of s_2

We can calculate the second marginal moment of the single step PDF $s_2(t, t_a)$ directly in the time domain. For this we need the stepping rate $k(t) = C_0(t)$, whose behavior depends on whether $\gamma > 1$ or $\gamma < 1$.

$\gamma < 1$

In this case we find by inverse transform of C_0 from table 4.1:

$$k(t) = \frac{1}{\Gamma(\gamma)\Gamma(1-\gamma)} t_0^{-\gamma} t^{\gamma-1} = \frac{\sin \pi\gamma}{\pi} t_0^{-\gamma} t^{\gamma-1}, \quad (4.72)$$

where the Γ product formula was used for the second equality. Inserting this result into the general formula Eq. (4.52) we find

$$s_2(t, t_a) = \gamma \frac{\sin(\pi\gamma)}{\pi} c^2 \int_0^{t_a} \int_{t_a+t-t'}^\infty [(t_a+t-t')^\eta - (t_a-t')^\eta]^2 \times (t')^{\gamma-1} (t'')^{2(\nu-\eta)} \frac{1}{(t_0+t'')^{\gamma+1}} dt'' dt'. \quad (4.73)$$

Just like r_2 in the ordinary case, this integral only converges for $\gamma > 2(\nu - \eta)$, meaning that η again governs the existence of the second moment. In the limit $t_0 \ll t''$ we can write:

$$s_2(t, t_a) \simeq \gamma \frac{\sin(\pi\gamma)}{\pi} \frac{1}{\gamma - 2(\nu - \eta)} c^2 \times \int_0^{t_a} (t_a+t-t')^{2(\nu-\eta)-\gamma} [(t_a+t-t')^\eta - (t_a-t')^\eta]^2 (t')^{\gamma-1} dt'. \quad (4.74)$$

The expression in square brackets is again approximated by $t^{2\eta}$ and (t_a+t-t') by its value at t , so that

$$s_2(t, t_a) \propto c^2 t_a^\gamma t^{2\nu-\gamma}. \quad (4.75)$$

$\gamma > 1$

In this regime we can use $k(t) = \frac{1}{\tau}$ again. Substituting this into Eq. (4.52) and approximating the term in square brackets results in

$$s_2(t, t_a) \simeq \gamma \frac{1}{\gamma - 2(\nu - \eta)} c^2 \frac{t_0^\gamma}{\tau} t^{2\eta} \int_0^{t_a} (t_a+t-t')^{2(\nu-\eta)-\gamma} dt', \quad (4.76)$$

which gives us

$$s_2(t, t_a) \simeq \gamma \frac{1}{(\gamma - 2(\nu - \eta))} c^2 \frac{t_0^\gamma}{\tau} t_a t^{2\nu-\gamma}. \quad (4.77)$$

The results so far are summarized in Table 4.2. Here we used the fact that $\tau \propto t_0$, see Eq. (4.5).

$\gamma < 1$	$F_0(s t_a) \simeq 1$	$F_2(s t_a) \propto \begin{cases} c^2 t_a^{2\nu} & \text{for } 2\nu < \gamma \\ c^2 t_a^\gamma s^{\gamma-2\nu} & \text{for } 2\nu > \gamma \end{cases}$
$\gamma < 1$		$s_2(t, t_a) \propto c^2 t_a^\gamma t^{2\nu-\gamma}$
$\gamma > 1$	$F_0(s t_a) \simeq 1$	$F_2(s t_a) \propto \begin{cases} c^2 t_0^{2\nu} & \text{for } 2\nu < \gamma - 1 \\ c^2 t_0^{\gamma-1} t_a^{2\nu+1-\gamma} & \text{for } \gamma - 1 < 2\nu < \gamma \\ c^2 t_0^{\gamma-1} t_a s^{\gamma-2\nu} & \text{for } 2\nu > \gamma \end{cases}$
$\gamma > 1$		$s_2(t, t_a) \simeq c^2 t_0^{\gamma-1} t_a t^{2\nu-\gamma}$

Table 4.2.: Results for F_0 and F_2 in the Laplace domain as well as s_2 in the time domain for different parameter ranges in the case of weak aging $t \gg t_a$. Dimensionless prefactors are omitted.

Mean squared displacement

We are now ready to calculate the MSD in the weakly aged case. Recall our earlier result

$$\begin{aligned} \langle x^2 \rangle(s|t_a) = & F_0(s|t_a)C_0(s)r_2(s) + F_0(s|t_a)C_2(s)r_0(s) \\ & + F_2(s|t_a)C_0(s)r_0(s) + s_2(s, t_a). \end{aligned} \quad (4.78)$$

We can now write down the first three terms in the Laplace domain using the results from the tables 4.1 and 4.2, and transform them back into the time domain. The last term in the time domain is already known. The calculation results in different asymptotics depending on γ .

$\gamma < 1$

In this regime the terms $F_0C_0r_2$ and $F_0C_2r_0$ reproduce the result for the non-aged walks. The term $F_2C_0r_0(s) \propto t_a^\gamma s^{\gamma-2\nu-1}$ translates into $F_2C_0r_0(t) \propto c^2 t^{2\nu} (t_a/t)^\gamma$, and is subdominant for $t \gg t_a$ for $2\nu > \gamma$. For $2\nu < \gamma$ this term tends to $const \cdot c^2 t_a^{2\nu} s^{-1}$, i.e. is a constant proportional to $c^2 t_a^{2\nu}$ in the time domain, and is again subdominant with respect to the previous terms. The term s_2 has the same asymptotics as the previous one in the first case, $s_2 \propto c^2 t^{2\nu} (t_a/t)^\gamma$ and therefore is also subdominant. The leading terms therefore behave as in the ordinary case.

$\gamma > 1$

For this regime the contributions $F_0C_0r_2$ and $F_0C_2r_0$ give the same behavior as in the non-aged case, $\propto t^{2\nu+1-\gamma}$ for $2\nu > \gamma$, or $\propto t$ in the opposite case. The contribution $F_2C_0r_0(s)$ either corresponds to $s^{\gamma-2\nu-1}$ and translates to $t^{2\nu-\gamma}$ for $2\nu > \gamma$, or to a

constant for $2\nu < \gamma$, and is always subdominant. The contribution of s_2 is always subdominant as well.

In conclusion we find that the behavior for short aging times reproduces the behavior of the ordinary walk in leading order up to prefactors, as one might expect, and has the same range of convergence: The MSD exists for $\gamma > 2(\nu - \eta)$.

4.4. MSD in the aged case: long aging times

Calculation of F_0 and F_2

We now consider the limit $t_a \gg t$. Here the cases $\gamma < 1$ and $\gamma > 1$ have to be distinguished again:

$$\gamma < 1$$

In this domain we can reuse the previous result in Eq.(4.53), but we now expand it for $t_a \gg t$:

$$F_0(t|t_a) = \frac{\sin \pi \gamma}{\pi} \left(\frac{t_a}{t} \right)^\gamma \frac{1}{t + t_a} \simeq \frac{\sin \pi \gamma}{\pi} t_a^{\gamma-1} t^{-\gamma}, \quad (4.79)$$

so that we get in the Laplace domain

$$F_0(s|t_a) \simeq \frac{\sin \pi \gamma}{\pi} \Gamma(1 - \gamma) t_a^{\gamma-1} s^{\gamma-1}. \quad (4.80)$$

For $F_2(t|t_a)$ we can use our result for $k(t)$, Eq.(4.72), and insert it into (4.49):

$$F_2(t|t_a) = \gamma \frac{\sin(\pi \gamma)}{\pi} c^2 \int_0^{t_a} (t_a + t - t')^{2(\nu-\eta)} [(t_a + t - t')^\eta - (t_a - t')^\eta]^2 \times \frac{(t')^{\gamma-1}}{(t_0 + t_a + t - t')^{1+\gamma}} dt'. \quad (4.81)$$

Neglecting t_0 in the expression in the last line this simplifies to

$$F_2(t|t_a) \simeq \gamma \frac{\sin(\pi \gamma)}{\pi} c^2 t_a^{2\nu-2} \int_0^{t_a} \left(1 + \frac{t}{t_a} - \frac{t'}{t_a} \right)^{2(\nu-\eta)-\gamma-1} \times \left[\left(1 + \frac{t}{t_a} - \frac{t'}{t_a} \right)^\eta - \left(1 - \frac{t'}{t_a} \right)^\eta \right]^2 \left(\frac{t'}{t_a} \right)^{\gamma-1} dt'. \quad (4.82)$$

We introduce the dimensionless variables $z = 1 - \frac{t'}{t_a}$ and $y = \frac{t}{t_a}$ and rewrite the integral as:

$$F_2(t|t_a) = \gamma \frac{\sin(\pi\gamma)}{\pi} c^2 t_a^{2\nu-1} \int_0^1 (z+y)^{2(\nu-\eta)-1-\gamma} [(z+y)^\eta - z^\eta]^2 (1-z)^{\gamma-1} dz. \quad (4.83)$$

Since we are going to encounter integrals of this type several times, we will calculate them separately. The general form

$$I_{a,b,c}(y) = \int_0^1 (z+y)^a [(z+y)^c - z^c]^2 (1-z)^b dz \quad (4.84)$$

can be expressed in terms of Gauss hypergeometric functions, leading to the following asymptotic behavior for $y \rightarrow 0$

$$I_{a,b,c}(y) \simeq \begin{cases} C(a,c) y^{1+a+2c} & \text{for } a+2c < 1 \\ B(1+b, a+2c-1) y^2 c^2 & \text{for } a+2c > 1. \end{cases} \quad (4.85)$$

A detailed derivation and the bounds for the constant $C(a,c)$ are given in Appendix B.

The behavior of F_2 follows with the substitutions $a = 2(\nu - \eta) - \gamma - 1$, $b = \gamma - 1$, $c = \eta$. Omitting dimensionless constants we obtain two distinct regimes in the limit $t_a \gg t$, depending on the relation between ν and γ :

$$F_2(t|t_a) \propto \begin{cases} c^2 t_a^{2\nu-3} t^2 & \text{for } 2\nu > \gamma + 2 \\ c^2 t_a^{\gamma-1} t^{2\nu-\gamma} & \text{for } 2\nu < \gamma + 2. \end{cases} \quad (4.86)$$

Since both of these cases belong to the non-integrable class, we obtain in the Laplace-domain:

$$F_2(s|t_a) \propto \begin{cases} c^2 t_a^{2\nu-3} s^{-3} & \text{for } 2\nu > \gamma + 2 \\ c^2 t_a^{\gamma-1} s^{\gamma-2\nu-1} & \text{for } 2\nu < \gamma + 2. \end{cases} \quad (4.87)$$

$\gamma > 1$

By substituting $k(t') = \tau^{-1}$ one finds

$$F_0 = \int_0^{t_a} \psi(t_a + t - t') \frac{1}{\tau} dt' \rightarrow \frac{1}{\tau} \Psi(t) \simeq \frac{t_0^\gamma}{\tau} t^{-\gamma}. \quad (4.88)$$

Since $\gamma > 1$, the term F_0 is of the integrable type, and therefore

$$F_0(s|t_a) \simeq \text{const.} \quad (4.89)$$

Now we turn to F_2 . Starting from equation (4.49) one finds

$$F_2(t|t_a) \simeq \gamma c^2 \frac{t_0^\gamma}{\tau} t_a^{2\nu-\gamma-1} \int_0^{t_a} \left(1 + \frac{t}{t_a} - \frac{t'}{t_a}\right)^{2(\nu-\eta)-\gamma-1} \times \left[\left(1 + \frac{t}{t_a} - \frac{t'}{t_a}\right)^\eta - \left(1 - \frac{t'}{t_a}\right)^\eta \right]^2 dt' . \quad (4.90)$$

The calculation is similar to the one in the case $\gamma < 1$. By applying Eq.(4.85) to $I_{2(\nu-\eta)-\gamma-1,0,\eta}(t/t_a)$ we obtain

$$F_2(t|t_a) \simeq \gamma c^2 \frac{t_0^\gamma}{\tau} \begin{cases} \eta^2 B(1, 2\nu - \gamma - 2) t_a^{2\nu-\gamma-2} t^2 & \text{for } 2\nu > \gamma + 2 \\ C \cdot t^{2\nu-\gamma} & \text{for } 2\nu < \gamma + 2. \end{cases} \quad (4.91)$$

The case $2\nu > \gamma + 2$ still belongs in the non-integrable class and therefore transforms into

$$F_2(s|t_a) \simeq 2\gamma \eta^2 B(1, 2\nu - \gamma - 2) c^2 \frac{t_0^\gamma}{\tau} t_a^{2\nu-\gamma-2} s^{-3}, \quad (4.92)$$

however for $2\nu < \gamma + 2$ we have to distinguish between $\gamma - 1 < 2\nu < \gamma + 2$, where the F_2 is non-integrable, and $2\nu < \gamma - 1$, where it is integrable. Therefore:

$$F_2(s|t_a) \simeq \gamma c^2 \frac{t_0^\gamma}{\tau} \begin{cases} \eta^2 B(1, 2\nu - \gamma - 2) t_a^{2\nu-\gamma-2} s^{-3} & 2\nu > \gamma + 2 \\ C \Gamma(2\nu + 1 - \gamma) s^{\gamma-2\nu-1} & \gamma + 2 > 2\nu > \gamma - 1 \\ \text{const } t_0^{2\nu+1-\gamma} & 2\nu < \gamma - 1. \end{cases} \quad (4.93)$$

Calculation of s_2

$\gamma < 1$

The calculations for s_2 from Eq. (4.52) are similar to that for F_2 case and yield

$$s_2(t, t_a) \simeq \gamma \frac{1}{\gamma - 2(\nu - \eta)} \frac{\sin(\pi\gamma)}{\pi} c^2 \quad (4.94)$$

$$\times \begin{cases} 2\eta^2 B(2\nu - \gamma - 1, \gamma) t_a^{2\nu-2} t^2 & \text{for } 2\nu > \gamma + 1 \\ C t_a^{\gamma-1} t^{2\nu+1-\gamma} & \text{for } 2\nu < \gamma + 1. \end{cases} \quad (4.95)$$

$\gamma > 1$

In this case we have

$$s_2(t, t_a) \simeq \gamma \frac{1}{\gamma - 2(\nu - \eta)} c^2 \frac{t_0^\gamma}{\tau} \int_0^{t_a} [(t_a + t - t')^\eta - (t_a - t')^\eta]^2 \times (t_a + t - t')^{2(\nu - \eta) - \gamma} dt' \quad (4.96)$$

$$= \gamma \frac{1}{\gamma - 2(\nu - \eta)} I_{2(\nu - \eta) - \gamma, 0, \eta} c^2 \frac{t_0^\gamma}{\tau} (t_a)^{2\nu + 1 - \gamma} \left(\frac{t}{t_a} \right). \quad (4.97)$$

Using Eq.(4.85) again we find

$$s_2(t, t_a) \simeq \gamma \frac{1}{\gamma - 2(\nu - \eta)} c^2 \frac{t_0^\gamma}{\tau} \times \begin{cases} \eta^2 B(2\nu - \gamma - 1, 1) t_a^{2\nu - \gamma - 1} t^2 & \text{for } 2\nu > \gamma + 1 \\ C t^{2\nu + 1 - \gamma} & \text{for } 2\nu < \gamma + 1. \end{cases} \quad (4.98)$$

The corresponding results for the case of long aging times are summarized in Table 4.3.

$\gamma < 1$	$F_0(s t_a) \propto t_a^{\gamma-1} s^{\gamma-1}$	$F_2(s t_a) \propto c^2 \begin{cases} t_a^{2\nu-3} s^{-3} & 2\nu > \gamma + 2 \\ t_a^{\gamma-1} s^{\gamma-2\nu-1} & 2\nu < \gamma + 2 \end{cases}$
$\gamma < 1$		$s_2(t, t_a) \propto c^2 \begin{cases} t_a^{2\nu-2} t^2 & 2\nu > \gamma + 1 \\ t_a^{\gamma-1} t^{2\nu+1-\gamma} & 2\nu < \gamma + 1 \end{cases}$
$\gamma > 1$	$F_0(s t_a) \propto 1$	$F_2(s t_a) \propto c^2 \begin{cases} t_0^{\gamma-1} t_a^{2\nu-\gamma-2} s^{-3} & 2\nu > \gamma + 2 \\ t_0^{\gamma-1} s^{\gamma-2\nu-1} & \gamma + 2 > 2\nu > \gamma - 1 \\ t_0^{2\nu} & 2\nu < \gamma - 1 \end{cases}$
$\gamma > 1$		$s_2(t, t_a) \propto c^2 \begin{cases} t_0^{\gamma-1} t_a^{2\nu-\gamma-1} t^2 & 2\nu > \gamma + 1 \\ t_0^{\gamma-1} t^{2\nu+1-\gamma} & 2\nu < \gamma + 1 \end{cases}$

Table 4.3.: Results for F_0 and F_2 in the Laplace domain as well as s_2 in the time domain for different parameter ranges in the case of long aging times $t_a \gg t \gg t_0$. Dimensionless prefactors are omitted.

Mean squared displacement

With these results we can now compute the MSD in the strongly aged case. Using Tables 4.1 and 4.3 we can write down the asymptotic behavior of the combinations $F_0 C_0 r_2$, $F_0 C_2 r_0$ and $F_2 C_0 r_0$ in the Laplace domain. The inverse transforms are then

performed using the Tauberian theorem. The corresponding results for $\gamma < 1$ and for $\gamma > 1$ are summarized in Tables 4.4 and 4.5.

Therefore for considerably aged walks we have:

	$F_2 C_0 r_0$	$F_0 C_0 r_2$	$F_0 C_2 r_0$	s_2
$2\nu < \gamma$	$c^2 t_a^{\gamma-1} t^{2\nu+1-\gamma}$	$c^2 t_a^{\gamma-1} t^{2\nu+1-\gamma}$	$c^2 t_0^{2\nu-\gamma} t_a^{\gamma-1} t$	$c^2 t_a^{\gamma-1} t^{2\nu+1-\gamma}$
$\gamma < 2\nu < 1 + \gamma$	$c^2 t_a^{\gamma-1} t^{2\nu+1-\gamma}$	$c^2 t_a^{\gamma-1} t^{2\nu+1-\gamma}$	$c^2 t_a^{\gamma-1} t^{2\nu+1-\gamma}$	$c^2 t_a^{\gamma-1} t^{2\nu+1-\gamma}$
$1 + \gamma < 2\nu < 2 + \gamma$	$c^2 t_a^{\gamma-1} t^{2\nu+1-\gamma}$	$c^2 t_a^{\gamma-1} t^{2\nu+1-\gamma}$	$c^2 t_a^{\gamma-1} t^{2\nu+1-\gamma}$	$c^2 t_a^{2\nu-2} t^2$
$2 + \gamma < 2\nu$	$c^2 t_a^{2\nu-3} t^3$	$c^2 t_a^{\gamma-1} t^{2\nu+1-\gamma}$	$c^2 t_a^{\gamma-1} t^{2\nu+1-\gamma}$	$c^2 t_a^{2\nu-2} t^2$

Table 4.4.: Asymptotic behavior of the contributions to the MSD for $\gamma < 1$ in the limit $t_a \gg t \gg t_0$. All dimensionless prefactors are omitted. The dominant terms are highlighted in boldface.

	$F_2 C_0 r_0$	$F_0 C_0 r_2$	$F_0 C_2 r_0$	s_2
$2\nu < \gamma - 1$	$c^2 t_0^{2\nu}$	$c^2 t_0^{2\nu}$	$c^2 t_0^{2\nu-1} t$	$c^2 t_0^{\gamma-1} t^{2\nu+1-\gamma}$
$\gamma - 1 < 2\nu < \gamma$	$c^2 t_0^{\gamma-1} t^{2\nu+1-\gamma}$	$c^2 t_0^{\gamma-1} t^{2\nu+1-\gamma}$	$c^2 t_0^{2\nu-1} t$	$c^2 t_0^{\gamma-1} t^{2\nu+1-\gamma}$
$\gamma < 2\nu < 1 + \gamma$	$c^2 t_0^{\gamma-1} t^{2\nu+1-\gamma}$	$c^2 t_0^{\gamma-1} t^{2\nu+1-\gamma}$	$c^2 t_0^{\gamma-1} t^{2\nu+1-\gamma}$	$c^2 t_0^{\gamma-1} t^{2\nu+1-\gamma}$
$1 + \gamma < 2\nu < 2 + \gamma$	$c^2 t_0^{\gamma-1} t^{2\nu+1-\gamma}$	$c^2 t_0^{\gamma-1} t^{2\nu+1-\gamma}$	$c^2 t_0^{\gamma-1} t^{2\nu+1-\gamma}$	$c^2 t_0^{\gamma-1} t_a^{2\nu-\gamma-1} t^2$
$2 + \gamma < 2\nu$	$c^2 t_0^{\gamma-1} t_a^{2\nu-\gamma-2} t^3$	$c^2 t_0^{\gamma-1} t^{2\nu+1-\gamma}$	$c^2 t_0^{\gamma-1} t^{2\nu+1-\gamma}$	$c^2 t_0^{\gamma-1} t_a^{2\nu-\gamma-1} t^2$

Table 4.5.: Asymptotic behavior of the contributions to the MSD for $\gamma > 1$ in the limit $t_a \gg t \gg t_0$. All dimensionless prefactors are omitted. The dominant terms are highlighted in boldface.

$\gamma < 1$:

$$\langle x^2(t) \rangle \propto \begin{cases} t_a^{\gamma-1} t & \text{for } 2\nu < \gamma \\ t_a^{\gamma-1} t^{2\nu+1-\gamma} & \text{for } \gamma < 2\nu < 1 + \gamma \\ t_a^{2\nu-2} t^2 & \text{for } 1 + \gamma < 2\nu. \end{cases} \quad (4.99)$$

$\gamma > 1$

$$\langle x^2(t) \rangle \propto \begin{cases} t & \text{for } 2\nu < \gamma \\ t^{2\nu+1-\gamma} & \text{for } \gamma < 2\nu < 1 + \gamma \\ t_a^{2\nu-\gamma-1} t^2 & \text{for } 1 + \gamma < 2\nu. \end{cases} \quad (4.100)$$

Therefore in the regime where the ordinary walk shows normal diffusion or enhanced diffusion there are no or weak changes due to aging (differing only by prefactor).

In the regime where the ordinary walk is superballistic, it ages to a ballistic one. This finding complies with the fact that a ballistic walk with $\nu = 1$ shows only weak aging, i.e. again the ballistic aged behavior [27, 28].

We also see that no Richardson superballistic regime $\langle x^2 \rangle \propto t^3$ is possible in the aged walk.

4.5. PDF in the ordinary case

The starting point for the calculation of the asymptotic behavior of the PDF will be the general result from Eq. (2.27)

$$p(\mathbf{k}|s) = \frac{r(\mathbf{k}|s)}{1 - \psi(\mathbf{k}, s)}. \quad (4.101)$$

While I was able to express $r(\mathbf{k}|s)$ and $\psi(\mathbf{k}, s)$ in terms of Fox H-functions (see [29] for definitions and properties) for arbitrary values of (\mathbf{k}, s) the resulting expression does not lend itself to performing the inverse Fourier transform.

So instead I will again focus on the one dimensional case and expand $r(k, s)$ and $\psi(k, s)$ for small k (corresponding to large x) as in the calculation for the MSD, which are of the form

$$r(k, s) \simeq r_0(s) - \frac{k^2}{2} r_2(s) \quad (4.102)$$

$$\psi(k, s) \simeq \psi_0(s) - \frac{k^2}{2} \psi_2(s). \quad (4.103)$$

Inserting this into the PDF we obtain

$$p(k|s) \simeq \frac{r_0(s) - \frac{k^2}{2} r_2(s)}{1 - (\psi_0(s) - \frac{k^2}{2} \psi_2(s))}. \quad (4.104)$$

From the results for $\psi_0(s)$ in Eqs. (4.3) and (4.4) and the fact that the marginal distributions are all positive it follows that the PDF in Fourier Laplace space takes the

general form

$$p(k|s) = \frac{A - Bk^2}{C + Dk^2}, \quad (4.105)$$

where A , B , C and D are all positive numbers that depend on s but not on k and which are defined as:

$$A = r_0(s); \quad B = \frac{1}{2}r_2(s); \quad C = 1 - \psi_0(s); \quad D = \frac{1}{2}\psi_2(s). \quad (4.106)$$

The inverse Fourier transform was defined as

$$p(k|s) = \frac{1}{2\pi} \int_{-\infty}^{\infty} \frac{A - Bk^2}{C + Dk^2} e^{-ikx} dk, \quad (4.107)$$

which can be computed using the residue theorem: There are two simple poles, $k = \pm i\sqrt{\frac{C}{D}}$ and depending on whether $x > 0$ or $x < 0$ we can close the contour over lower or the upper half of the complex plain respectively. Combining the two cases we find

$$p(x|s) = \frac{1}{2} \frac{A + \frac{BC}{D}}{\sqrt{DC}} e^{-\sqrt{\frac{C}{D}}|x|}, \quad (4.108)$$

The s dependence can now be found by inserting the previous results for r , which are summarized in Table 4.1, and the results for ψ which are found in Eqs. (4.3), (4.4), (4.10) and (4.11). Here a number of cases have to be considered separately:

$2\nu < 1$ **and** $\gamma < 2\nu$

In this regime I obtain

$$p(x|s) \propto \frac{s^{\gamma-1} + \frac{s^{\gamma-1-2\nu}s^\gamma}{s^{\gamma-2\nu}}}{\sqrt{s^{\gamma-2\nu}s^\gamma}} e^{-s^\nu|x|} \quad (4.109)$$

$$\propto s^{\nu-1} e^{-s^\nu|x|}. \quad (4.110)$$

$2\nu < 1$ **and** $2\nu < \gamma < 1$

Here I find

$$p(x|s) \propto \frac{s^{\gamma-1} + \frac{s^{\gamma-1-2\nu}s^\gamma}{1}}{\sqrt{s^\gamma 1}} e^{-|x|s^{\gamma/2}} \quad (4.111)$$

$$\simeq s^{\gamma/2-1} e^{-|x|s^{\gamma/2}}. \quad (4.112)$$

$2\nu < 1$ **and** $1 < \gamma < 1 + 2\nu$

For these parameters the PDF becomes

$$p(x|s) \propto \frac{1 + \frac{s^{\gamma-1-2\nu}s}{1}}{\sqrt{s^{1-1}}} e^{-|x|s^{1/2}} \quad (4.113)$$

$$\simeq s^{-1/2} e^{-|x|s^{1/2}}. \quad (4.114)$$

$2\nu < 1$ **and** $1 + 2\nu < \gamma$

Here we have

$$p(x|s) \propto \frac{1 + \frac{s}{1}}{\sqrt{s^{\gamma/2-1}}} e^{-|x|s^{1/2}} \quad (4.115)$$

$$\simeq s^{-1/2} e^{-|x|s^{1/2}}, \quad (4.116)$$

which is identical to the previous case.

$1 < 2\nu$ **and** $1 < \gamma < 2\nu$

In this case the PDF takes the form

$$p(x|s) \propto \frac{1 + \frac{s^{\gamma-2\nu}}{s^{\gamma-2\nu}}}{\sqrt{s^{\gamma-2\nu}s}} e^{-|x|s^{(2\nu-\gamma+1)/2}} \quad (4.117)$$

$$\simeq s^{(2\nu-\gamma-1)/2} e^{-|x|s^{(2\nu-\gamma+1)/2}}. \quad (4.118)$$

All other cases with $1 < 2\nu$ reduce to the ones we have already considered. In total we notice that the PDF is always of the form

$$p(x|s) \simeq s^{\alpha-1} e^{-|x|s^\alpha}, \quad (4.119)$$

where the values of α in the different parameter regions are summarized in Fig. 4.1. There is no known solution for the inverse Laplace transform of this expression for general values of α . However for the special case of $\alpha = \frac{1}{2}$ the result is known to be

$$p(x|t) = \frac{1}{\sqrt{\pi t}} e^{-\frac{1}{4t}|x|^2}, \quad (4.120)$$

i.e. a Gaussian distribution with variance $\sqrt{2t}$.

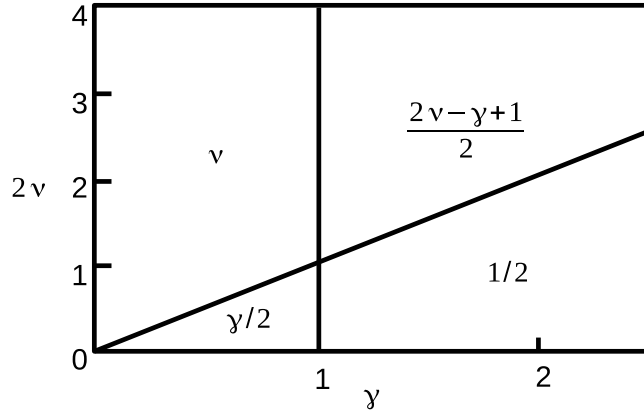


Figure 4.1.: Values of α in the different regions of parameter space. Solid lines correspond to changes in the regime.

For the similar one-sided alpha-stable Lévy distribution, whose Laplace transform reads

$$f(s) = e^{-s^\alpha}, \quad (4.121)$$

there exists a closed expression for all rational $\alpha < 1$ derived in [30], where the result is expressed in generalized hypergeometric functions. This can be related to our case via the Riemann-Liouville fractional derivative of order $\alpha - 1$ [29]. Unfortunately I was not able to find a closed expression for this result that could be evaluated.

However the second factor $e^{-|x|s^\alpha}$ is always slowly varying in the limit $s \rightarrow 0$, therefore the Tauberian theorem in Eq. (3.18) tells us that the leading order of the inverse Laplace transformation will be proportional to $t^{-\alpha}$. While this loses the exact dependence on $|x|$, it does predict how the PDF will depend on time at the origin $|x| = 0$, which can be compared to the results of the simulation.

We can furthermore evaluate the inverse transform numerically, using the algorithm developed by Talbot [23], which I mentioned earlier. The results of this are presented in Sec. 5.6.

5. Results and Discussion

5.1. Ordinary MSD

The results for the MSD in the ordinary case in one dimension found in Eq. 4.46 are summarized in Fig. 5.1 (taken from [15]). We see that sub- as well as superdiffusion

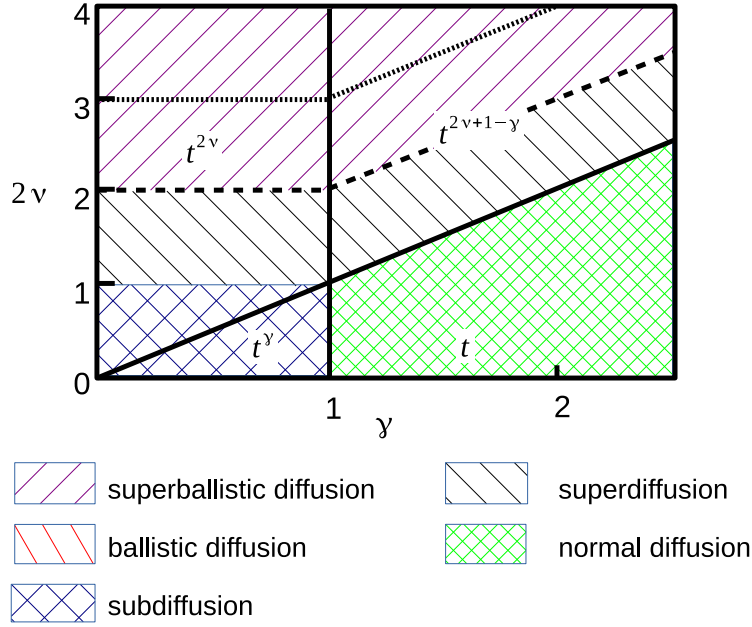


Figure 5.1.: The picture shows the asymptotic time dependence of the ensemble average $\langle x^2 \rangle \propto t^x$ in the ordinary Lévy walk. The thick solid lines correspond to the changes in time exponent while the hatchings indicate the type of diffusion. The dashed line corresponds to ballistic behavior and the dotted one to the Richardson law.

are realized in the ordinary case, and that we can even reach superballistic diffusion for large values of η . This includes the Richardson regime, which is achieved for $\nu = 3/2$ for $\gamma < 1$, and for $\nu = (\gamma + 2)/2$ for $\gamma > 1$.

Also note that the region of normal diffusion is confined to the parameter ranges of $\gamma > 1$, $2\nu < \gamma$. This corresponds to a finite step duration and finite mean squared step length, which means the asymptotic PDF is subject to the central limit theorem. We therefore expect normal diffusion in this region, which is confirmed by the results shown here.

We also see that the new parameter η does not affect the time dependence but only the prefactor in leading order. Instead it governs the divergence that arises when calculating the second marginal moment of the distribution of incomplete steps, $r_2(t)$. Here we rederive the condition of convergence found in [12], $\gamma > 2(\nu - \eta)$, which in the picture corresponds to the region below a diagonal line parallel to the bold one whose offset is given by 2η . Increasing η therefore increases the domain of finite MSD in the picture, with $\nu = \eta$ always resulting in a finite MSD. From this we can see that for the original model with $\eta = 1$ the Richardson regime is found either over or exactly on the line, and is therefore divergent.

These results were tested through simulations, with an ensemble of 10^5 particles. To ensure that the particles had time to reach the asymptotic behavior of $t \gg t_0$ the last observation time was set to $t_{max} = 20000 t_0$ ¹. I have then fitted the simulation results with $f(x) = a x^b$, where b corresponds to the time exponent from the analytical calculations. We see in Fig. 5.2 that the MSD indeed follows a power law, with the time exponent being in good agreement with the analytic predictions. This was tested further, with various configurations of γ , ν and η , and the deviation from the predicted exponent was always smaller than 0.04. These small deviation can be explained by the influence of subleading terms for finite t_{max} . The simulation therefore confirms the results of the analytical calculation.

¹All times are multiples of t_0 , which was set to 1 in the simulation. Similarly all lengths are multiples of ct_0'' , which is also set to 1.

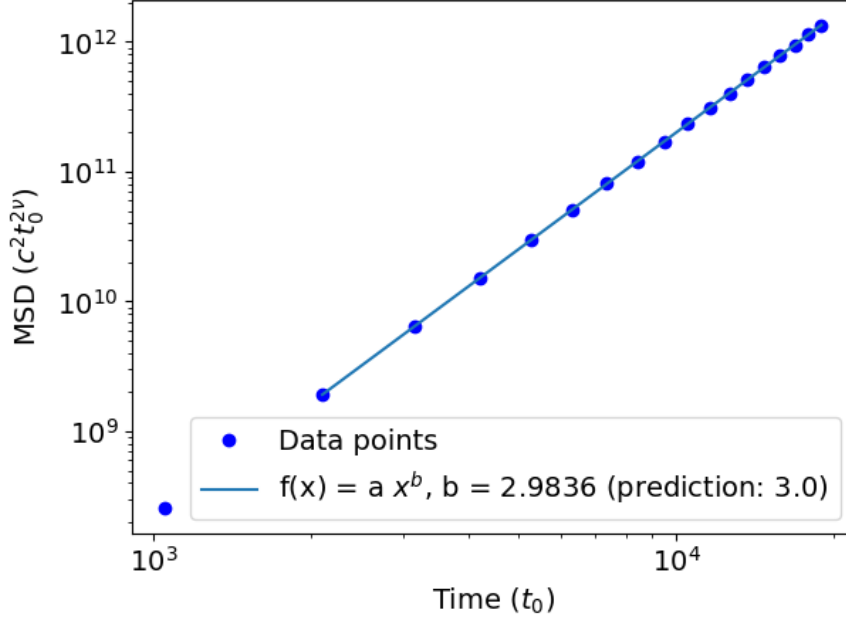


Figure 5.2.: Fit of the time dependence for the ordinary MSD in the case $\gamma = 0.6$, $\nu = 1.5$ and $\eta = 1.7$ ($\chi^2 = 0.01$).

5.2. Aged MSD

For short aging times we reproduce the behavior of the ordinary walk in leading order up to prefactors, which is to be expected as the ordinary and aged results should coincide in the limit of $t_a \rightarrow 0$. We also find that, in addition to $r_2(t)$, there is now a second possibly divergent contribution from $s_2(t)$, but both terms have the same condition of convergence as the ordinary case, $\gamma > 2(\nu - \eta)$.

For long aging times the behavior of the walker differs significantly, which is illustrated in Fig. 5.3 (taken from [15]). We see that for the parameter range where the ordinary walk showed subdiffusion we now find regular diffusion, but with a prefactor that decays with growing aging times. There is no longer any superballistic diffusion and thus no Richardson regime. However this does not make the model unsuitable for the description of the Richardson regime, since that relates to measuring the distance between two tracers immediately after they have been released into a stationary flow, i.e. corresponds to the ordinary case.

Furthermore we see that the aging has no effect on the parameter region with finite mean step duration ($\gamma > 1$) wherever the ordinary walk showed normal or superdiffusive behavior ($2\nu < \gamma + 1$).

The results for convergence are similar to the previous cases, in that the second moment only exists for $\gamma > 2(\nu - \eta)$. Where the MSD exists the value of η only enters the

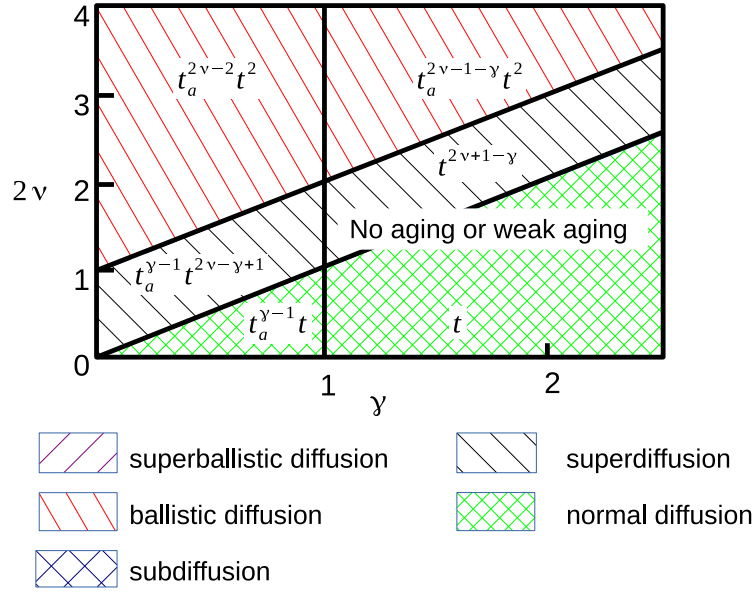


Figure 5.3.: The panel shows the asymptotic behavior of the ensemble average $\langle x^2(t) \rangle$ for the Lévy walk in the limit of long aging times. The thick solid lines correspond to the changes in time-dependence while the hatchings represent the different types of diffusion.

prefactors, and does not change the asymptotic power law dependence of the MSD, similar to the ordinary case.

It is noteworthy that the highest possible time exponent in the aged walk is quadratic, which seems counterintuitive, because for long aging times the ensemble is dominated by steps whose duration is much longer than the observation time, and whose contribution to the MSD should scale with t^ν . So why can the walker not move faster than ballistic diffusion?

The answer is not that the walker somehow moves slower in the aged case, but instead this is caused by the first order approximation we make with regards to the observation time: Consider a walker whose step begins long before the beginning of observation at $-t_a$ and continues until the end of observation at t . His squared displacement during the observation is given by

$$|x|^2 = [c(t_a + t)^\nu - c(t_a + t)^{\nu-\eta}(t_a)^\eta]^2 \quad (5.1)$$

$$\simeq c^2 \eta^2 (t_a + t)^{2\nu-2\eta} t_a^{2\eta-2} t^2 \quad (5.2)$$

$$\simeq c^2 \eta^2 t_a^{2\nu-2} t^2, \quad (5.3)$$

which is exactly the result we see found for the parameter region $2\nu > \gamma + 1$ where such contributions dominate. The high speed of these walkers is just shifted from the t dependence to the prefactor, which scales with t_a . This is similar to the way previously

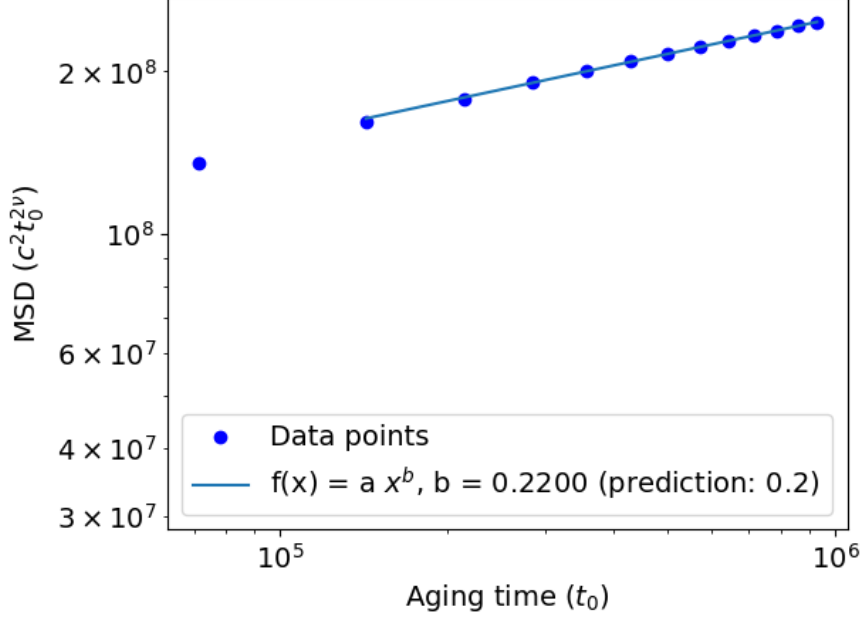


Figure 5.4.: Fit of the aging time dependence for the aged MSD in the case $\gamma = 0.8$, $\nu = 1.1$ and $\eta = 1.1$ ($\chi^2 = 2.88$).

subdiffusive parameter ranges, which now show normal diffusion, have a prefactor that decreases with larger aging times.

We moreover note that the double time-ensemble average $\langle \langle x^2(t) \rangle_T \rangle_E$, also discussed in Ref. [12], whose calculation involves an additional integration over the time, $\langle \langle x^2(t) \rangle_T \rangle_E \simeq (T - t)^{-1} \int_0^{T-t} \langle x^2(t|t_a) \rangle dt_a$, shows the same behavior as the aged walk, if the measurement time t is associated with the time lag in the double average, and the aging time t_a is changed for the data acquisition time T .

The verification via the simulation now involves the fitting of the MSD with regards to the observation time as well as the aging time. Compared to the ordinary case considerably longer simulation times are needed, as both $t \gg t_0$ and $t_a \gg t$ have to be satisfied to reach the asymptotic limit. For an ensemble of 10^5 walkers with $t_{max} = 5 \cdot 10^3 t_0$ and $t_{a,max} = 10^6 t_0$ the aging time exponent is in good agreement with the analytical prediction, as can be seen in Fig. 5.4. The analytical results have again been tested for various configurations of γ , η and ν with the highest deviation of the aging time exponent from the analytic result being 0.06, which is again caused by the finite duration of the simulation.

5.3. Simulation of the PDF in the ordinary case

The PDF was investigated numerically in one dimension by generating histograms for large ensembles of 10^9 walkers. Since the PDF is symmetric, only the positive side is shown in the following figures. Unlike the MSD, where the new parameter η only

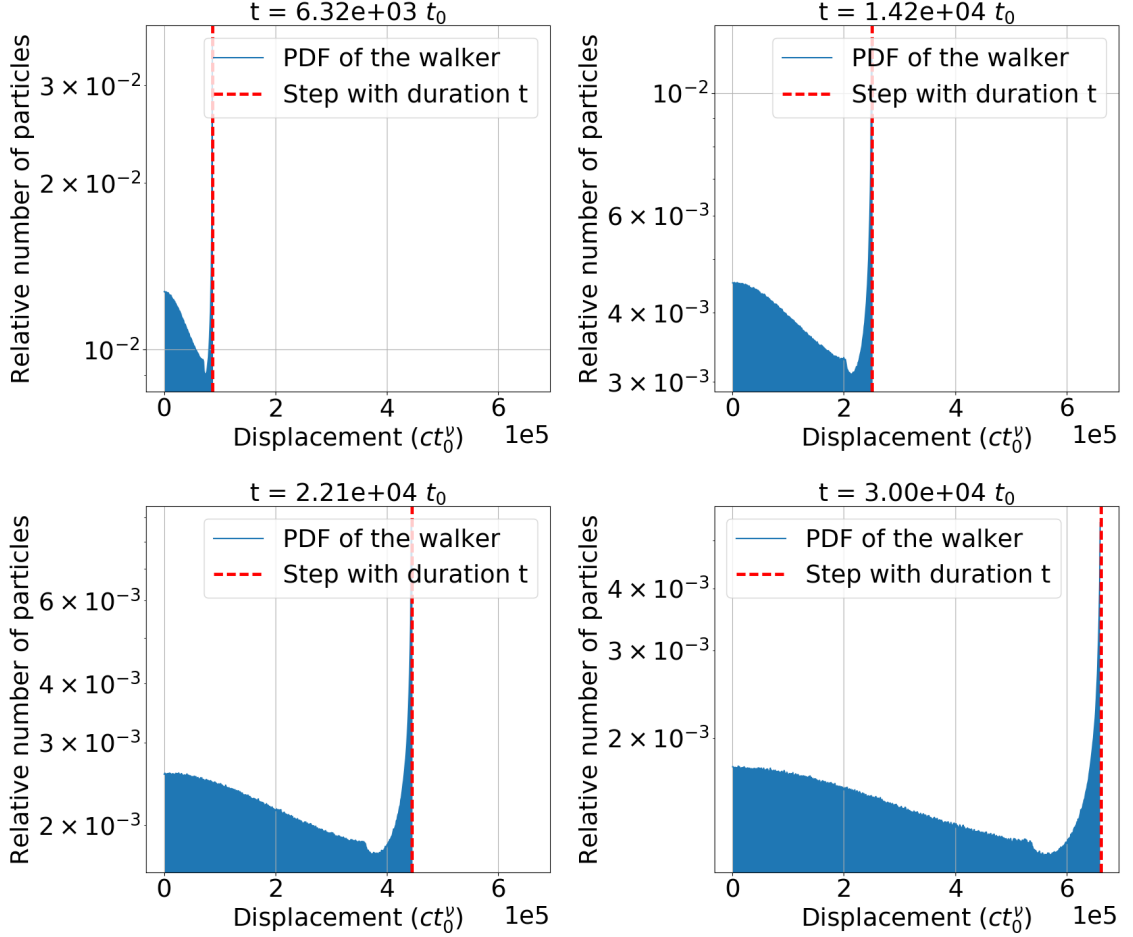


Figure 5.5.: Histograms of a Lévy walk with $\gamma = 0.6$, $\nu = 1.3$ and $\eta = 1.3$ at different points in time. The dashed line indicates the position a walker would have reached in a single step beginning at $t = 0$ and ending exactly at the time of the respective panel.

changes the prefactors of finite results, η has a major impact on the shape of the PDF: In the case $\nu = \eta$, shown in Fig. 5.5, the histogram has a clear cutoff marked by a delta peak with a continuous left flank, which coincides with the position a walker can reach in a single step of duration t . This is similar to what you find for the related velocity model ($\eta = \nu = 1$), where the PDF also has a clear boundary behind which no

walker can be found [7].

This can be understood by considering the displacement in the first step of a walk,

$$|\mathbf{x}_1| = ct_1^{\nu-\eta}t^\eta, \quad (5.4)$$

where we recall that t_1 is the total duration of the step, which may be longer than the observation time t . In the case of $\eta = \nu$ the dependence on the total step duration vanishes, which means that any particle starting at $t = 0$ moves with the same speed, regardless of how long the total step duration is. Since $\eta > 1$ the greatest displacement is archived when the particle performs a single step whose duration is greater or equal than the observation time. This means two things: Firstly, no particle can be found beyond this limit, and secondly, the entire probability of having a step duration of t or longer is concentrated on this particular cutoff, which explains the delta peak in the histograms.

Besides the peak we see the highest probability density at the origin, which then seems to decays exponentially with the distance from the origin, $p \propto e^{-|x|}$. Directly before the peak a minor notch can be seen in the histogram, whose origin is unclear.

However this shape of the PDF changes profoundly when modifying η , as can be seen in Fig 5.6: Here both γ and ν are identical to the previous picture, but η is now smaller than ν . Now walkers travel well beyond the limit of what can be reached in a single step of total duration t , and there is no longer a delta peak. Instead the dashed line marks the distinction between a simple exponential decay close to the origin and a faster decay further away.

This shape can again be understood by considering Eq. (5.4): Because we have $\eta < \nu$ the first factor of the displacement now grows with the total step duration. This means that walkers whose step duration is larger than the observation time can reach arbitrarily high initial velocities and therefore move well beyond the dashed line. Consequently the walker has a finite probability to be at any point for $t > 0$, which is not fully captured here, since the histogram only covers a finite range, and the positions of walkers that move beyond the histogram range cannot be shown.

Also note that while very long steps are not extremely rare (the mean step duration diverges in the case $\gamma < 1$), for finite ensembles these outliers are nevertheless hard to capture and even with 10^9 walkers we see the limits of the simulation in the edges of the PDF, where it becomes discontinuous.

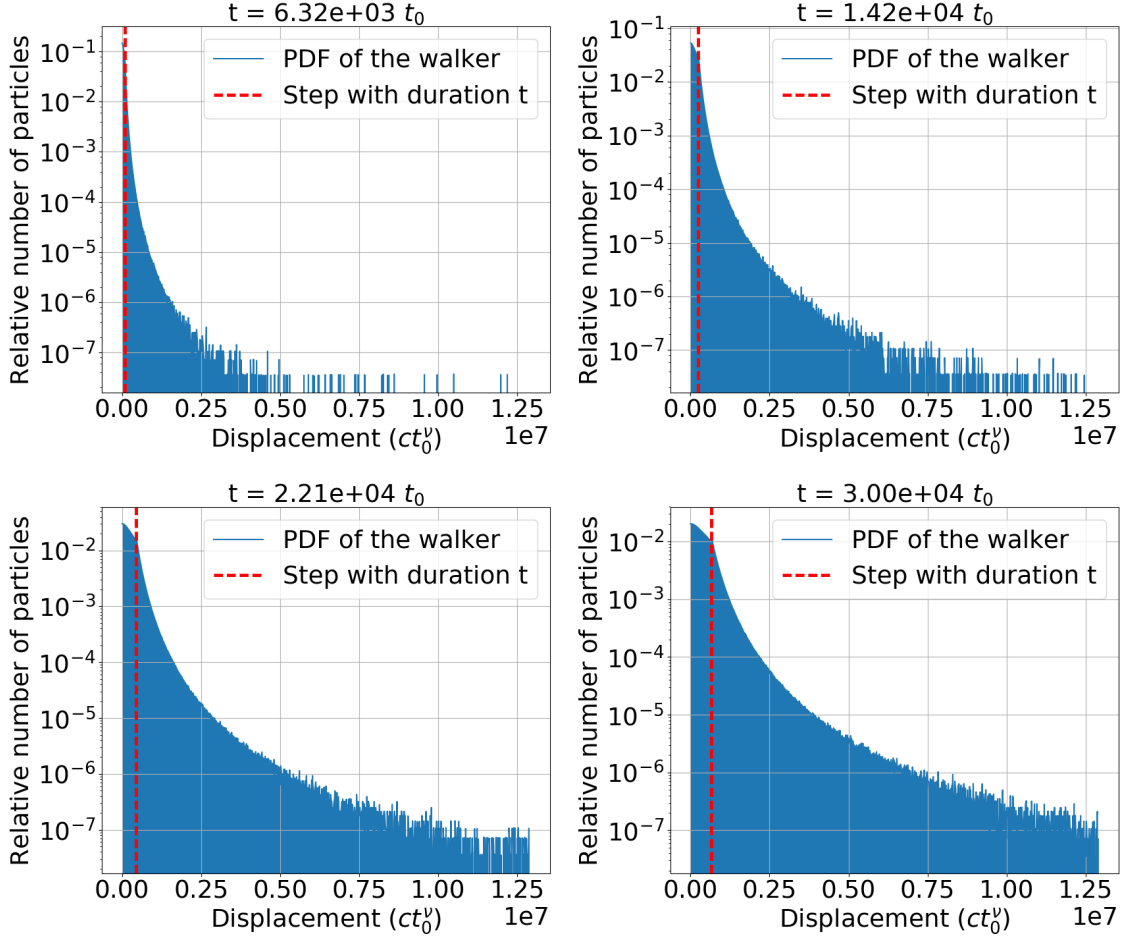


Figure 5.6.: Histograms of a Lévy walk with $\gamma = 0.6$, $\nu = 1.3$ and $\eta = 1.1$ at different points in time. The dashed line indicates the position a walker would have reached in a single step beginning at $t = 0$ and ending exactly at the time of the respective panel.

Moving on to the case of $\eta > \nu$, which is shown in Fig. 5.7, we see that the shape of the PDF is again different: Similar to the $\eta = \nu$ case the dashed line marks a clear limit of how far a walker can reach, but there is no delta peak. Inspecting Eq. (5.4) again we see the reason: Because we have $\eta > \nu$ the prefactor in the displacement actually becomes smaller with increasing total step duration, meaning that any walker performing a step with duration longer than t cannot reach the cutoff. Therefore only walkers with a step duration of exactly t can arrive at the dashed line, the probability of which is infinitesimal.

These findings explain the convergence condition we rederived for the MSD, $\gamma > 2(\nu - \eta)$: For $\eta \geq \nu$ the support of the PDF is bounded, and therefore the MSD always converges.

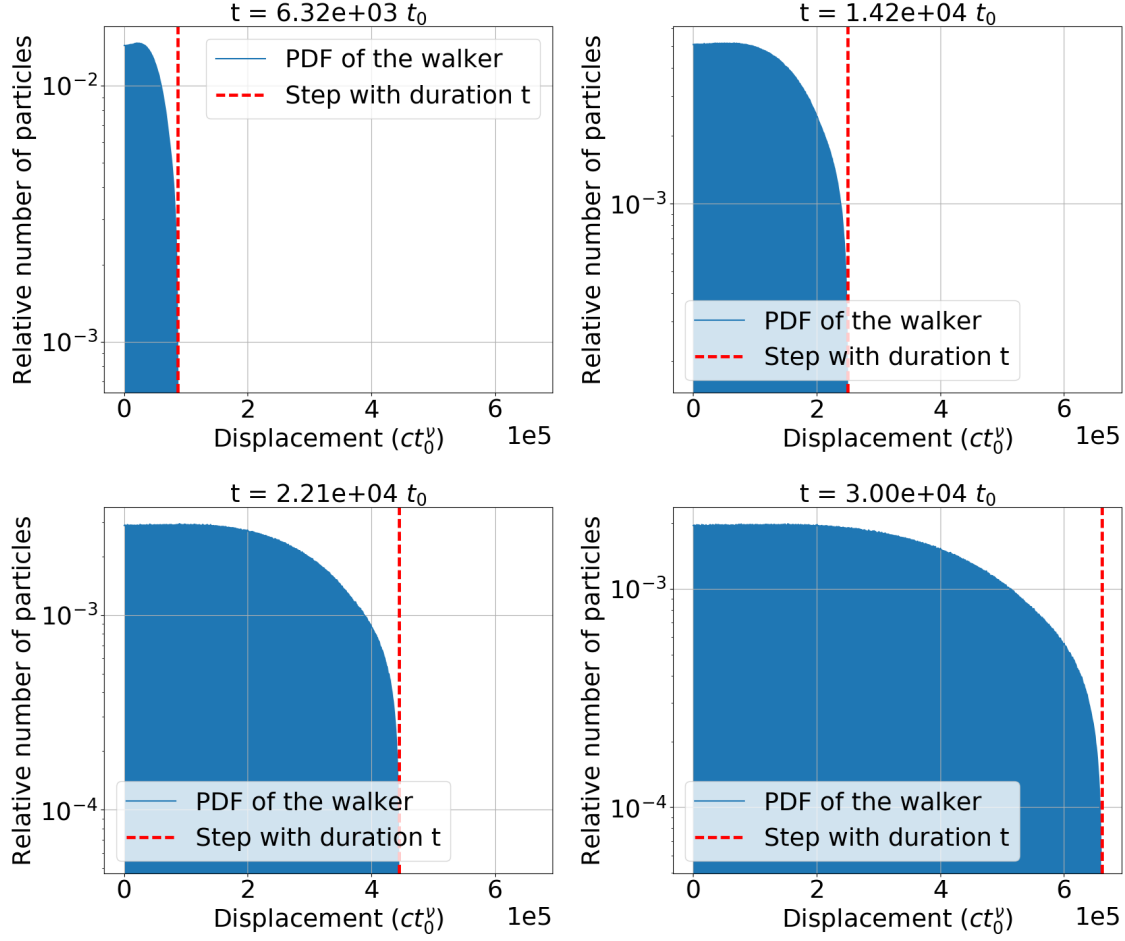


Figure 5.7.: Histograms of a Lévy walk with $\gamma = 0.6$, $\nu = 1.3$ and $\eta = 1.5$ at different points in time. The dashed line indicates the position a walker would have reached in a single step beginning at $t = 0$ and ending exactly at the time of the respective panel.

For $\eta < \nu$ this is no longer the case and there is a finite probability to find the walker at any distance from the origin for $t > 0$. Convergence now depends on the likelihood of extreme events, meaning that γ has to be sufficiently large for the MSD to exist.

Next we are interested in the influence of the parameter ν on the shape of the PDF, which is illustrated in Fig. 5.8: We are again in the case of $\eta = \nu$, but unlike in Fig. 5.5 the dashed line no longer marks a sharp cutoff for the PDF, as there is a finite probability for a walker to be found beyond it. However this is not due to steps with durations longer than the observation time (all these cases reach exactly the boundary and contribute to the peak), but instead due to walkers that take more than one step: Since $\nu < 1$ the maximum displacement is not realized by making a single long step,

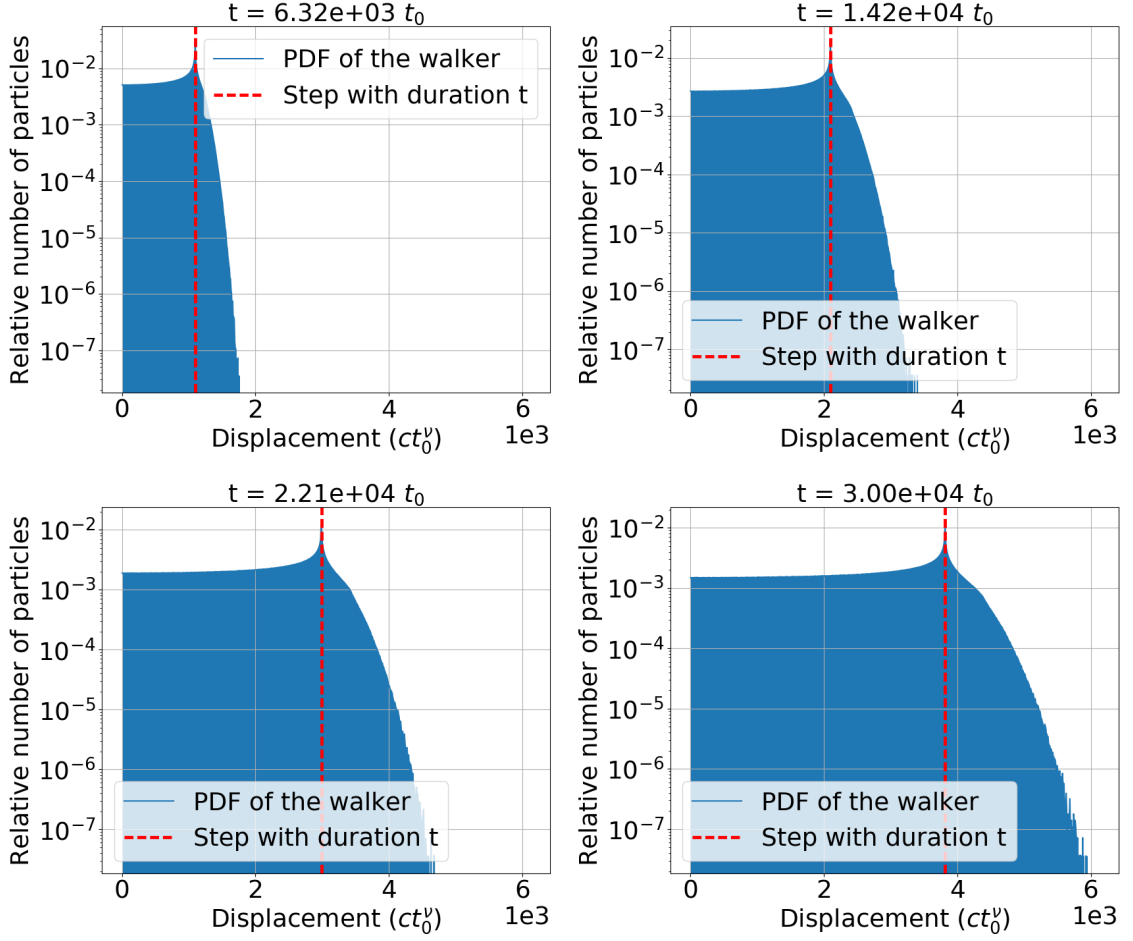


Figure 5.8.: Histograms of a Lévy walk with $\gamma = 0.6$, $\nu = 0.8$ and $\eta = 0.8$ at different points in time. The dashed line indicates the position a walker would have reached in a single step beginning at $t = 0$ and ending exactly at the time of the respective panel.

but rather by taking many smaller steps in the same direction, simply because the sum of a root is larger than the root of a sum. It follows, that values of $\nu < 1$ cause the breakdown of the sharp cutoff, and the simulations show that this effect becomes more pronounced with smaller η . However this kind of unboundedness does not cause a divergence of the MSD, because so many steps in the same direction are almost never realized for a power law step distributions.

Furthermore we consider the effect of varying γ on the PDF, which is shown in in Fig. 5.9. Comparing this to Fig. 5.5, which differs only in its γ value, we see that the peak is much less prominent, but the position of the cutoff does not change. Furthermore we see that the PDF is much more centered on the origin. This makes sense, as a

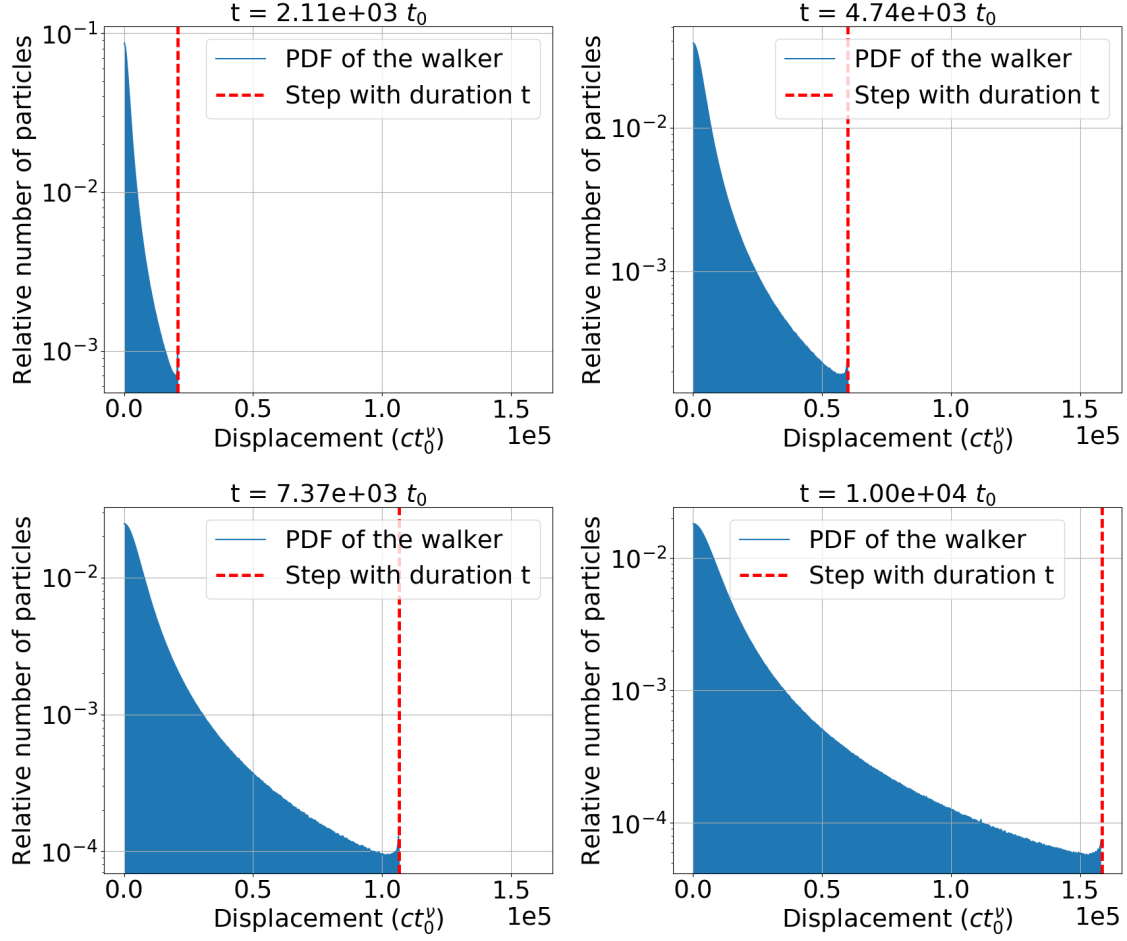


Figure 5.9.: Histograms of a Lévy walk with $\gamma = 1.2$, $\nu = 1.3$ and $\eta = 1.3$ at different points in time. The dashed line indicates the position a walker would have reached in a single step beginning at $t = 0$ and ending exactly at the time of the respective panel.

larger value of γ makes steps longer than the observation time much less likely, and the walk is therefore less dominated by these extreme events, which would be contributing to the height of the delta peak.

Finally we are interested in the case where both the mean step duration as well as the variance of the step length exist ($\gamma > 1$, $\gamma > 2\nu$). As can be seen in Fig. 5.10 the PDF takes the form of a Gaussian in this regime, as is predicted by the central limit theorem. The Gaussian is not bounded by a single step displacement, because $\nu < 1$ holds, as explained above. Unlike the previous cases this result is independent of the value of η .

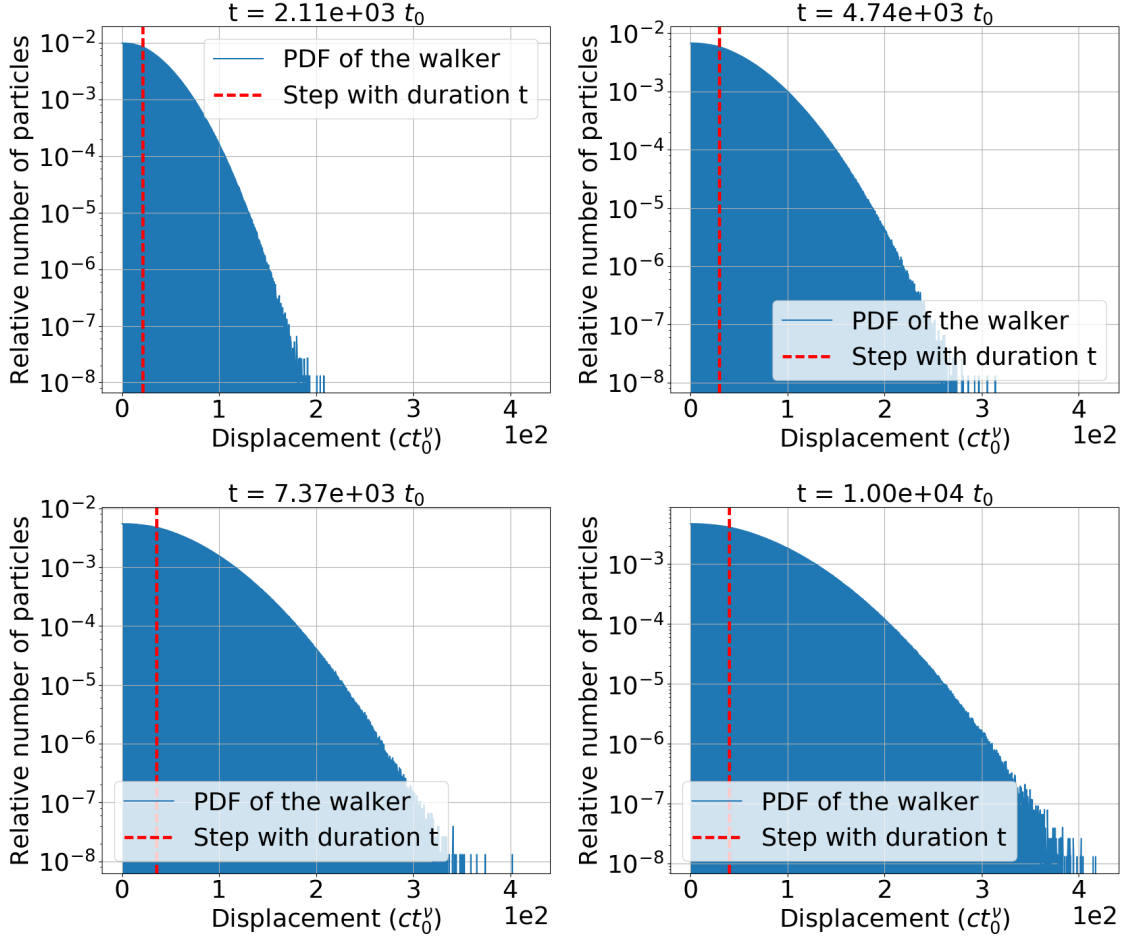


Figure 5.10.: Histograms of a Lévy walk with $\gamma = 1.2$, $\nu = 0.4$ and $\eta = 0.4$ at different points in time. The dashed line indicates the position a walker would have reached in a single step beginning at $t = 0$ and ending exactly at the time of the respective panel.

5.4. Simulation of the PDF in the aged case

The PDF of the generalized Lévy walk changes considerably under aging. An example of this for the case $\nu = \eta$ is shown in Fig. 5.11, where we can observe two jumps in the PDF, as opposed to one in the ordinary case, which correspond to two different events: The red line denotes the distance covered by a step starting at the beginning of observation and ending precisely at t , the second, yellow line corresponds to a step that started at $-t_a$ and ends at t .

Left of the dashed red line the probability density is comparatively small, as this region captures only events that had a change time since the beginning of observation, which is exceedingly rare for growing t_a . This is because the rate of steps decreases with time

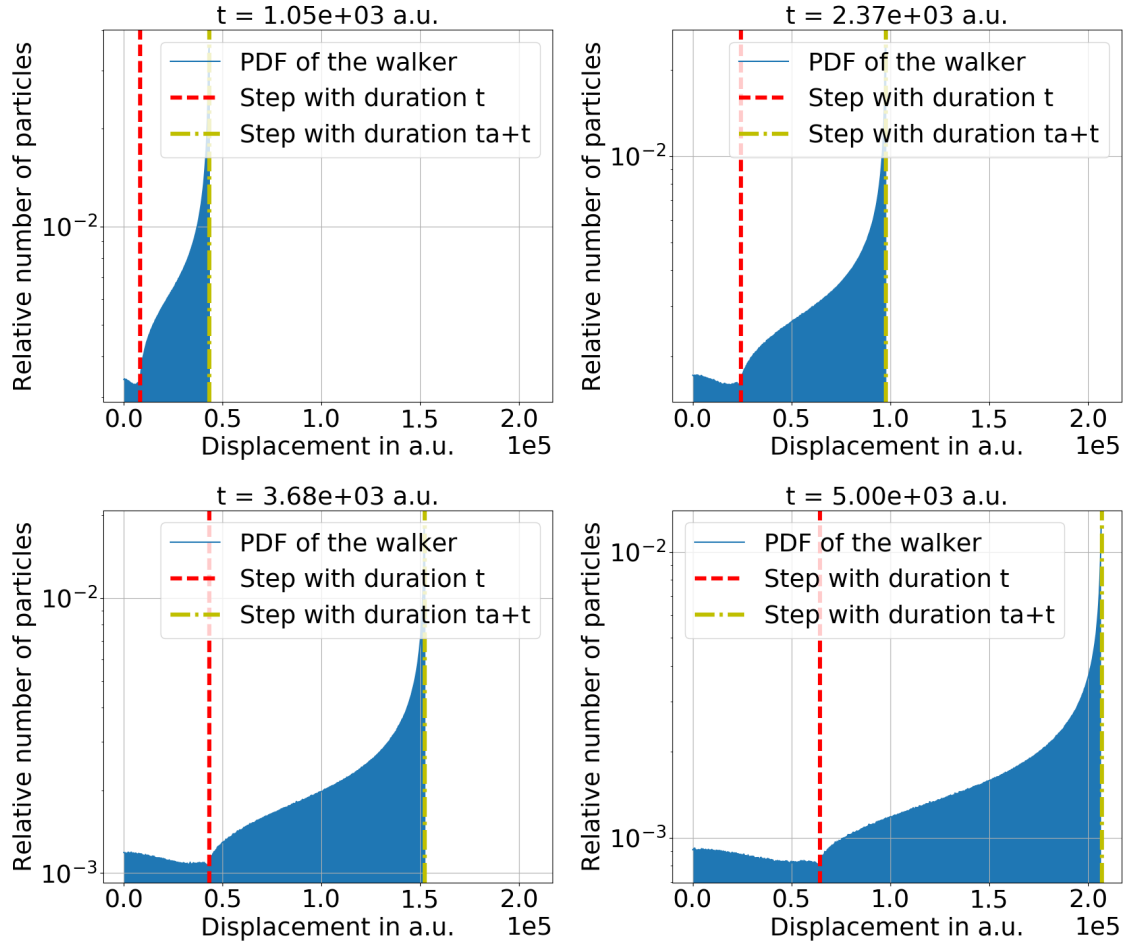


Figure 5.11.: Histograms of an aged Lévy walk with $\gamma = 0.6$, $\nu = 1.3$ and $\eta = 1.3$ and aging time $t_a = 10^5 t_0$ at different observation times. The dashed line indicates the position a walker would have reached in a single step beginning at $t = 0$ and ending exactly at the time of the respective panel. The dotted line indicates the displacement a step could archive during the observation, if it starts at $-t_a$ and ends at t .

for $\gamma < 1$, as discussed in Sec. 2.2.3.

Behind the red line the PDF increases rapidly, due to the contributions from walkers that spend the observation time in a single step. The upper limit here is given by walkers whose steps started at $-t_a$, which is indicated by the green line. Similar to the ordinary case we see a delta peak with a left flank here. This peak captures the probability of all cases that started at $-t_a$ and whose total step duration is equal or longer than $t_a + t$. Also note that the probability to find the particle at the origin is actually pretty small compared to the peak at maximum displacement. This is again caused by the large number of particles that are already locked into long steps at the beginning of observation. The effect of varying η in the aged case is similar to that

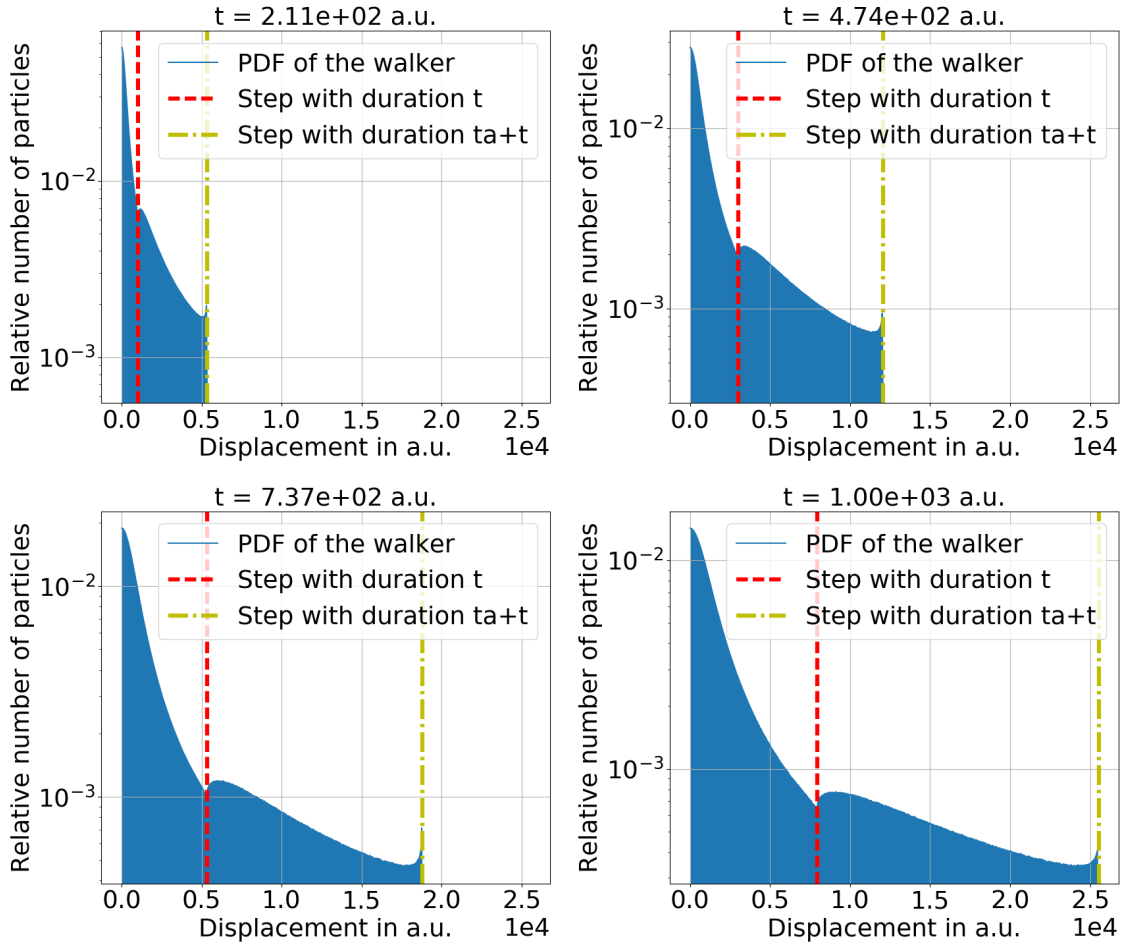


Figure 5.12.: Histograms of an aged Lévy walk with $\gamma = 1.1$, $\nu = 1.3$ and $\eta = 1.3$ and aging time $t_a = 2 \cdot 10^4 t_0$ at different observation times. The dashed line indicates the position a walker would have reached in a single step beginning at $t = 0$ and ending exactly at the time of the respective panel. The yellow line indicates the displacement a step could archive during the observation, if it starts at $-t_a$ and ends at t .

found in the ordinary case: For $\eta > \nu$ the peak vanishes and the probability to reach the second line becomes infinitesimal. For $\eta < \nu$ the yellow line no longer restricts the PDF, as the walker can now reach arbitrary distances.

Increasing the value of γ reduces the influence of very long stretches on the overall distribution, which manifests itself in less pronounced peaks and a PDF that is more concentrated around the origin, which is shown in Fig. 5.12.

However something interesting happens when we enter the regime $\nu < 1$, which is depicted in Fig. 5.13.

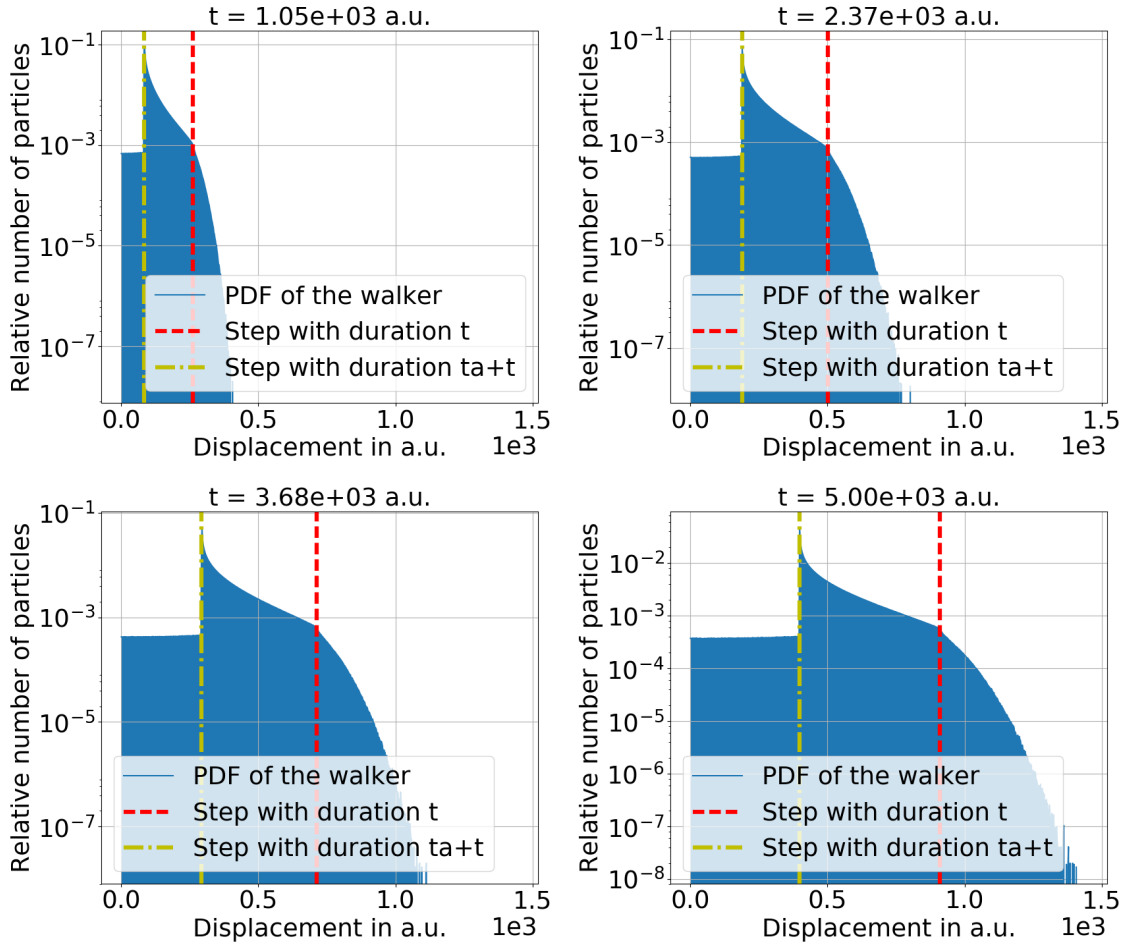


Figure 5.13.: Histograms of an aged Lévy walk with $\gamma = 0.6$, $\nu = 0.8$ and $\eta = 0.8$ and aging time $t_a = 10^5 t_0$ at different observation times. The dashed line indicates the position a walker would have reached in a single step beginning at $t = 0$ and ending exactly at the time of the respective panel. The yellow line indicates the displacement a step could archive during the observation, if it starts at $-t_a$ and ends at t .

We see that the yellow line is now closer to the origin than the red one, the reason for this being that the longest step durations no longer correspond to the largest displacements for $\nu < 1$. Directly at the yellow line the PDF forms a peak, due to the large number of walkers that have only performed one step so far. The flank of this peak is continuous on the right side, as these cases correspond to walkers that have also entered a very long step, but only slightly after the process began to age. Events left of the peak belong to walkers that reached a change point and changed directions during the observation, thus causing a smaller displacement from the origin. Further to the right we find the red dashed line, marking a sharper decrease in the flank of the PDF. As in the ordinary case with $\nu < 1$ walkers can move beyond this line by performing multiple steps in the same direction during observation, but this gets exceedingly rare, and the probability density falls off quickly.

5.5. Probability density at the origin

During the analytical approximation of the PDF in Sec. 4.5 we derived a prediction for the time dependence of the probability density at the origin, which is tested in the simulation. The results of the analytical calculation are shown in Fig. 5.14. By

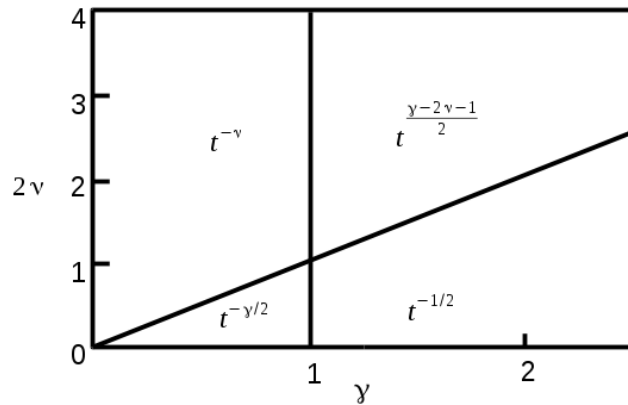


Figure 5.14.: The time dependence of the probability density for different values of the parameters ν and γ is shown. Thick lines indicate the distinction between two different regimes.

plotting the change in the PDF at the origin over a period double logarithmically we can extract the time exponent, as is shown in Fig. 5.15. We see that the PDF is indeed of the form t^x , and the deviation of the time exponent from the expected result, $t^{-0.55}$, is small. Fits with various other parameters confirm this result, with deviations always being smaller than 0.02

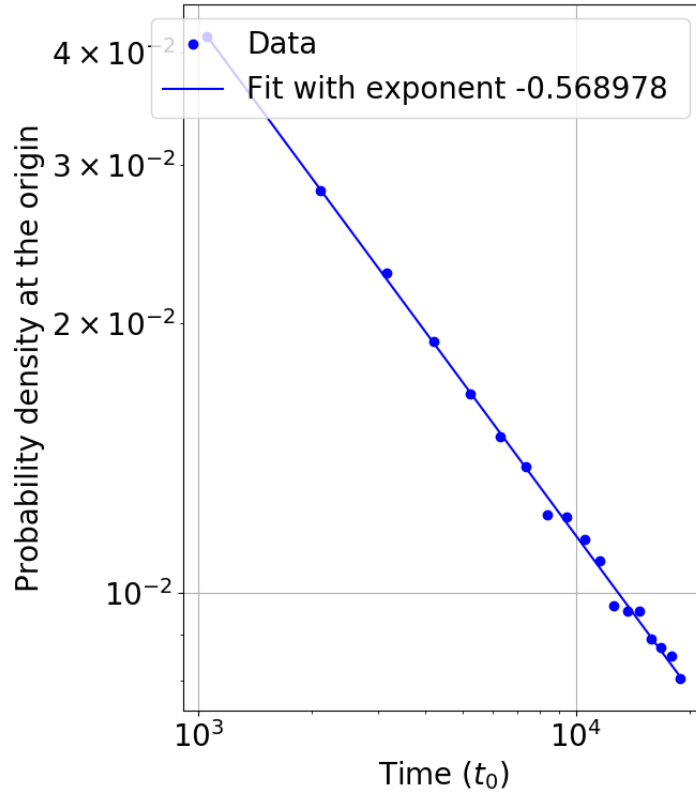


Figure 5.15.: The time dependence of the probability density for the parameter values $\gamma = 1.5$, $\nu = 0.8$ and $\eta = 0.8$ is shown. It is fitted with $f(x) = ax^b$ ($\chi^2 = 0.12$).

5.6. Analytic results for the PDF

We now turn our attention to the approximation for the PDF derived in Sec. 4.5. Here we found that the Laplace transform of the PDF takes the general form

$$p(x, s) \propto s^{\alpha-1} e^{-|x|s^\alpha} \quad (5.5)$$

with the values of alpha for the different regimes shown in Fig. 4.1.

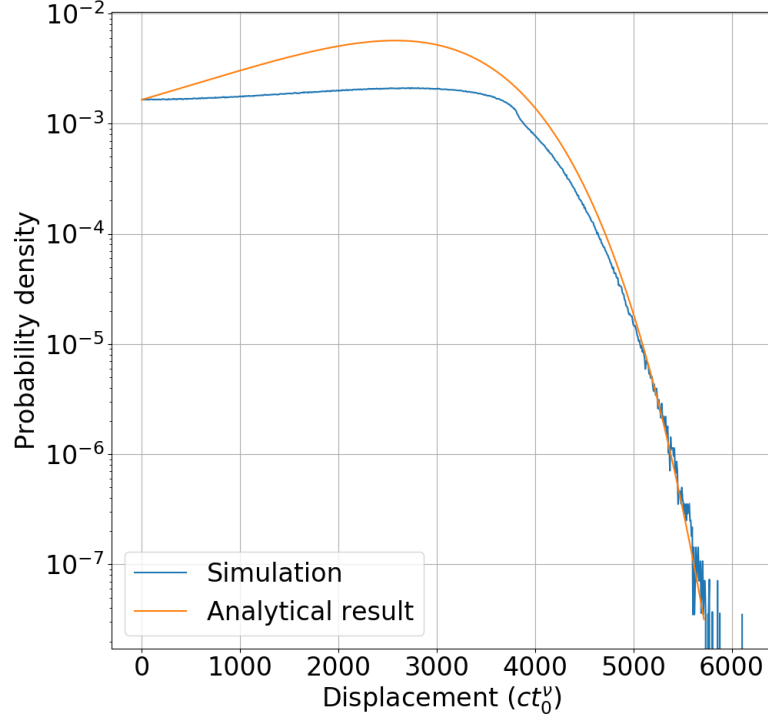


Figure 5.16.: Comparison of the histogram obtained in a simulation with $\gamma = 0.6$, $\nu = 0.8$ and $\eta = 1$ with the corresponding rescaled semi-analytic result for $\alpha = 0.8$.

Through numerical evaluation of the inverse Laplace transform we obtain a semi-analytic result for the PDF which in the case of $\alpha = 0.8$ is compared to the corresponding simulation in Fig. 5.16.

Since the prefactors of the semi-analytic result were lost in the calculation, the length scale and overall height of the expression were rescaled to match that of the simulation. While the behavior for large displacements is somewhat similar we see that, despite the rescaling, the semi-analytic result is not in good agreement with the simulation, with the initial slope being very different. The contrast is even more clear when one varies the value of η , which we found to have a considerable influence on the shape of the PDF, but does not impact the analytic expression. Comparisons with different values of α , which are not shown here, give a similar result. This is caused by the approximation made in the calculation, where r and ψ were expanded to second order, which we know from the calculation of the MSD does not depend on η in the asymptotic limit. This is fine for the MSD, whose time exponent is indeed independent of η , but for the PDF this approach misses much of the rich behavior seen in Sec. 5.3.

However the approximation is not completely off: As we have seen in the previous section, the prediction for the time dependence of the PDF at the origin is accurate,

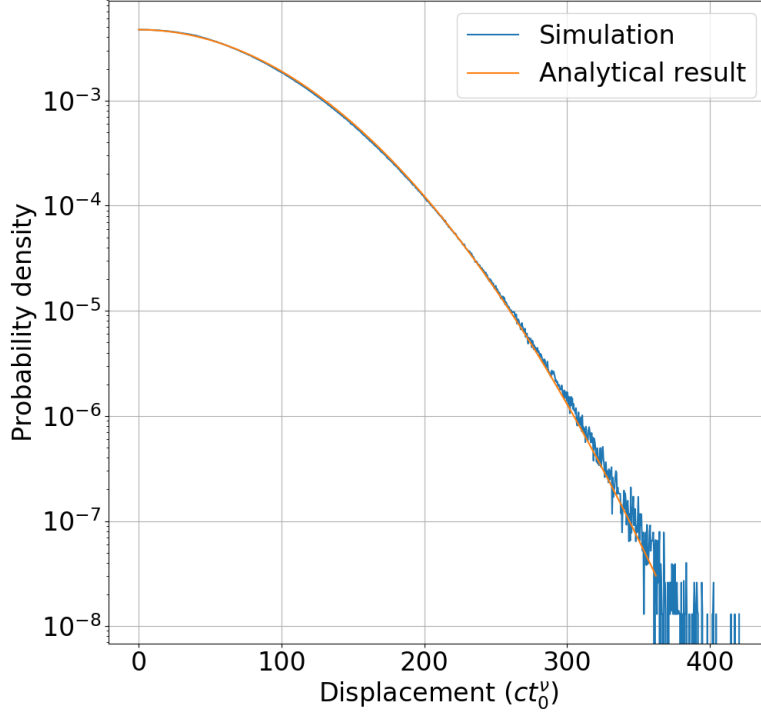


Figure 5.17.: Comparison of the histogram obtained in a simulation with $\gamma = 1.2$, $\nu = 0.4$ and $\eta = 0.4$ with the corresponding rescaled analytic result for $\alpha = 0.5$.

and it also correctly predicts the parameter region where the PDF tends to a Gaussian, which corresponds to $\alpha = 1/2$ (see Fig. 4.1). Here the simulated PDF loses its dependence on η and the two results match, as is depicted in Fig. 5.17.

6. Conclusions

The main question in this thesis was, how the introduction of a new acceleration parameter η into the widely used Lévy walk model changes its properties, and in particular what its effect on the recently found divergence in the MSD of the Lévy walk are.

To this end the asymptotic behavior of the MSD was calculated in one dimension, both for the ordinary and for the aged walk, which can be found in [15]. We showed that the MSD is finite when the condition $\gamma > 2(\nu - \eta)$ is satisfied, not just in the ordinary case, where this was already known [12], but for the aged case as well. This means that the introduction of η is indeed suitable to avoid the divergence of the original model. Furthermore we found that η does not affect the asymptotic time dependence of the MSD, meaning that for the ordinary walk, all diffusion regimes can be recovered from the original model for suitable values of η , including the superballistic Richardson regime.

Additionally it was discovered that in the limit of long aging times neither subdiffusion nor superballistic diffusion can be found in the generalized model.

A similar calculation attempted to find the asymptotic behavior of the PDF, but this could unfortunately not be done analytically for general parameter values. It was however possible to extract the correct time dependence of the probability density at the origin and to derive the analytical solution in the domain of applicability of the central limit theorem. For the other cases a numerical evaluation of the expression resulted in an approximation of the PDF that was not able to capture the rich behavior revealed in a simulation of the process.

For this simulation CUDA parallel computing was used to validate the findings for the MSD, and to create histograms for both the aged and the ordinary case. Here we find significant differences in the PDF for different values of the parameters γ and ν . Interestingly the new parameter η also has a major influence on the PDF, as it governs the formation of delta peaks as well as the existence of a cutoff for the PDF, which explains η 's role in the convergence condition discussed above. The results can mostly be explained heuristically by analyzing the influence of long steps on the process. We also find significant aging effects for the PDF, which can be explained by a similar analysis.

A goal for future work is to find an analytical expression that can describe the features of the PDF quantitatively. One approach could be the incorporation of higher order terms into the asymptotic expansion in this work, which can be done straightforwardly. It is however not immediately clear if this would capture the effect of η on the PDF, so another approach might be more suitable.

It should also be noted that this thesis focuses very much on the theoretical aspects of the model, so it should be studied how the different values of η could be realized in experimental settings. A natural candidate would be the case $\eta = \nu = 2$, corresponding to a process with constant acceleration, which has already been investigated for a similar model in [31, 32].

To summarize, we show that the generalized Lévy walk does indeed allow for the recovery of the diffusion regimes that were divergent in the original model. Furthermore we find that the introduction of η has a significant impact on the PDF, which should be investigated further.

A. The Tauberian theorem

In this thesis we frequently consider Laplace transforms of functions asymptotically following power laws. The asymptotic form of Laplace transforms of functions which at long times behave as $f(t) = t^{\rho-1}L(t)$, where $L(t)$ is a slowly varying function, in the asymptotic regime $s \rightarrow 0$ as well as the corresponding inverse transforms may be obtained by use of the Tauberian theorem. Note that the this derivation follows the calculation in [15].

We assume that a Laplace transform $f(s) = \int_0^\infty f(t)e^{-st}dt$ exists, i.e. the function $f(t)$ does not possess a strong divergence at 0. All functions $f(t)$ appearing this thesis are non-negative. For such functions Laplace transforms are monotonically decaying functions of s . Depending on the behavior of $f(t)$ at infinity two cases should be considered:

The function $f(t)$ might be integrable on $[0, \infty)$, so that $\int_0^\infty f(t)dt = I_0^f < \infty$, or this integral may diverge. The first case corresponds to $\rho < 0$ and the second one to $\rho > 0$ (the case $\rho = 0$ may belong to the either class depending on the concrete form of $L(t)$). In the second case the Tauberian theorem may be applied immediately, stating that if $f(t)$ is a regularly varying function, i.e. when its Laplace transform is given by

$$f(t) \simeq t^{\rho-1}L(t) \leftrightarrow f(s) \simeq \Gamma(\rho)s^{-\rho}L\left(\frac{1}{s}\right) \quad (\text{A.1})$$

for $\rho \geq 0$. As in the main text, all slowly varying functions will be omitted (i.e. changed for constants L).

We note that for $\rho < 0$ equation, i.e. when $f(t)$ is integrable, equation (A.1) suggests $f(s)$ being a growing function of s and is therefore wrong. In this case let us consider the function

$$S(t) = \int_t^\infty f(t')dt'. \quad (\text{A.2})$$

The integrability of $f(t)$ means that $S(t)$ is well-defined, and that $I_0^f = \int_0^\infty f(t')dt' = S(0)$ is finite. The function $S(t)$ has the power-law asymptotics

$$S(t) \simeq -\frac{Lt^\rho}{\rho}, \quad (\text{A.3})$$

and, if this is no more integrable (i.e. for $\rho > -1$), can be transformed via the Tauberian theorem, so that

$$S(s) \simeq -L \frac{\Gamma(\rho+1)}{\rho} s^{-(\rho+1)} = -L\Gamma(\rho) s^{-(\rho+1)}, \quad (\text{A.4})$$

where in the last equality the identity $\Gamma(x+1) = x\Gamma(x)$ was used. Noting that $f(t) = -\frac{d}{dt}S(t)$ and using the Laplace representation of the derivative, we get

$$f(s) = S(t=0) - sS(s) = I_0^f - L\Gamma(\rho) s^{-\rho}. \quad (\text{A.5})$$

The direct application of the Tauberian theorem would give us a correct form of the second term (up to a sign), but omit the first one.

If $S(t)$ is still integrable, we consider the function $P(t) = \int_t^\infty S(t') dt'$, whose power-law asymptotics for $t \rightarrow \infty$ is

$$P(t) \simeq \frac{Lt^{\rho+1}}{\rho(\rho+1)}, \quad (\text{A.6})$$

and whose connection to $f(t)$ is given by $f(t) = \frac{d^2}{dt^2}S(t)$. For $-2 < \rho$ the function $P(t)$ is not integrable, and the application of the Tauberian theorem gives

$$P(s) = L \frac{\Gamma(\rho+2)}{\rho(\rho+1)} s^{-\rho-2} = L\Gamma(\rho) s^{-\rho-2}. \quad (\text{A.7})$$

Using the Laplace representation for the second derivative we get

$$f(s) = -sP(t=0) - P'(t=0) + s^2P(s). \quad (\text{A.8})$$

The value of $P'(t=0)$ is $-S(t=0) = -I_0^f$. The value $P(t=0)$ is given by the integral

$$P(t=0) = \int_0^\infty dt \int_t^\infty f(t') dt'. \quad (\text{A.9})$$

Changing the sequence of integrations in t and t' we get

$$P(t=0) = \int_0^\infty dt' f(t') \int_0^{t'} dt = \int_0^\infty t' f(t') dt'. \quad (\text{A.10})$$

Since $f(t)$ decays with t faster than t^{-2} , the integral converges, and will be denoted by I_1^f . Therefore we have

$$f(s) = I_0^f - sI_1^f + L\Gamma(\rho) s^{-\rho}. \quad (\text{A.11})$$

For $\rho < -2$ the procedure has to be repeated again for the function being the integral

of $P(t)$, etc. The general result is

$$f(s) = \sum_{k=0}^{k_{\max}} \frac{(-1)^k}{k!} I_k^f s^k + L\Gamma(\rho) s^{-\rho} \quad (\text{A.12})$$

with k_{\max} being the whole part of $-\rho$, and I_k^f being the moment integral

$$I_k^f = \int_0^\infty t^k f(t) dt. \quad (\text{A.13})$$

In the main text we never have to use more than first three terms of this expansion.

B. Estimates for the integral $I_{a,b,c}(y)$

We are interested in the integral

$$\begin{aligned} I_{a,b,c}(y) &= \int_0^1 (1-z)^b [(z+y)^c - z^c]^2 (z+y)^a dz \\ &= \int_0^1 (1-z)^b \left[(z+y)^{a+2c} - 2(z+y)^{a+c} z^c + (z+y)^a z^{2c} \right] dz \end{aligned} \quad (\text{B.1})$$

in the limit of small $y = \frac{t}{t_a} \ll 1$ for the parameter ranges $c > 0$, $b > -1$, $a \in \mathbb{R}$, which was originally calculated in the appendix of [15].

To evaluate it we use Euler's integral representation for the Gauß hypergeometric function for $\Re c' > \Re b' > 0$

$${}_2F_1(a', b'; c'; x) = \frac{1}{\text{B}(b', c' - b')} \int_0^1 z^{b'-1} (1-z)^{c'-b'-1} (1-zx)^{-a'} dz. \quad (\text{B.2})$$

As the existence condition $1 + b > 0$ is always satisfied for all three terms in (B.1) we can write the integral as

$$\begin{aligned} I_{a,b,c}(y) &= y^a \left[y^{2c} \text{B}(1, 1+b) {}_2F_1 \left(-a-2c, 1; 2+b; -\frac{1}{y} \right) \right. \\ &\quad - 2y^c \text{B}(1+c, 1+b) {}_2F_1 \left(-a-c, 1+c; 2+b+c; -\frac{1}{y} \right) \\ &\quad \left. + \text{B}(1+2c, 1+b) {}_2F_1 \left(-a, 1+2c; 2+b+2c; -\frac{1}{y} \right) \right] \end{aligned} \quad (\text{B.3})$$

with $\text{B}(x, y)$ being the Beta function. Although the integral can be expressed in terms of three Gauß hypergeometric functions, its investigation is somewhat tricky, since the asymptotic regimes appear as a subleading terms in a sum of three large contributions whose leading terms cancel. First, to avoid evaluating hypergeometric functions at

$-\infty$ we make use of the Pfaff transformations:

$${}_2F_1(a', b'; c'; z) = (1 - z)^{-b'} {}_2F_1\left(b', c' - a'; c; \frac{z}{z - 1}\right) \quad (\text{B.4})$$

$${}_2F_1(a', b'; c'; z) = (1 - z)^{-a'} {}_2F_1\left(a', c' - b'; c; \frac{z}{z - 1}\right). \quad (\text{B.5})$$

These two forms will be applicable in different domains of parameters. Under the transformations the argument of the corresponding functions on the r.h.s., equal to $\frac{1}{1+y}$, will tend to 1. Applying the Pfaff transformation Eq.(B.4) to the integrals in Eq.(B.3) we find:

$$\begin{aligned} I_{a,b,c}(y) = & y^{1+a+2c} \\ & \times \left[(1+y)^{-1} \text{B}(1, 1+b) {}_2F_1\left(1, 2+a+b+2c; 2+b; \frac{1}{1+y}\right) \right. \\ & - 2(1+y)^{-1-c} \text{B}(1+c, 1+b) {}_2F_1\left(1+c, 2+a+b+2c; 2+b+c; \frac{1}{1+y}\right) \\ & \left. + (1+y)^{-1-2c} \text{B}(1+2c, 1+b) {}_2F_1\left(1+2c, 2+a+b+2c; 2+b+2c; \frac{1}{1+y}\right) \right]. \end{aligned}$$

We now use the Euler integral representation (B.2) again, but exchange the roles of a' and b' :

$${}_2F_1(a', b'; c'; x) = \frac{1}{\text{B}(a', c' - a')} \int_0^1 z^{a'-1} (1-z)^{c'-a'-1} (1-zx)^{-b'} dz$$

for $\Re c' > \Re a' > 0$. Note that the existence condition for the integrals is the same as before, $b+1 > 0$, which is satisfied for all cases relevant in this thesis, so we can write:

$$\begin{aligned} I_{a,b,c}(y) = & y^{1+a+2c} \int_0^1 \left[(1+y)^{-1} (1-z)^b \left(1 - \frac{z}{1+y}\right)^{-2-a-b-2c} \right. \\ & - 2(1+y)^{-1-c} z^c (1-z)^b \left(1 - \frac{z}{1+y}\right)^{-2-a-b-2c} \\ & \left. + (1+y)^{-1-2c} z^{2c} (1-z)^b \left(1 - \frac{z}{1+y}\right)^{-2-a-b-2c} \right] dz. \end{aligned}$$

The integrals of each of three contributions in square brackets would diverge for $y \rightarrow 0$, but the integral of whole sum is convergent for $a+2c < 1$ since for $y \rightarrow 0$ the integrand tends to

$$(1 - 2z^c + z^{2c})(1-z)^{-2-a-2c} = (1-z^c)^2(1-z)^{-2-a-2c},$$

and the integral

$$C(a, c) = \int_0^1 (1 - z^c)^2 (1 - z)^{-2-a-2c} dz$$

of this expression converges in the range $a + 2c < 1$ (to prove the convergence it is enough to expand the first term in vicinity of $z = 1$). This integral cannot be expressed in terms of “simple” functions, but the (loose) bounds for it follow easily.

Let us find two constants $B > A > 0$ such that for all $0 < z < 1$

$$A(1 - z) < 1 - z^c < B(1 - z).$$

To do so consider the function

$$f(z) = \frac{1 - z^c}{1 - z},$$

with $f(0) = 1$ and with its limiting value at $z \rightarrow 1$ given by the l'Hôpital's rule $\lim_{z \rightarrow 1} = c$. Therefore the limit of the function at 1 is larger than its value at 0 when $c > 1$ and smaller than this value when $c < 1$. For $c = 1$ this function equals to unity identically.

Now we consider $c \neq 1$ and proceed to show that the function $f(z)$ is monotonically growing for $c > 1$ and monotonically decaying for $c < 1$. To show this it is enough to show that its derivative on $[0, 1]$ does not vanish. The derivative of the corresponding function is

$$f'(z) = \frac{1 - z^c + cz^c - cz^{c-1}}{(1 - z)^2},$$

and can only vanish when the numerator, $g(z) = 1 - z^c + cz^c - cz^{c-1}$, vanishes somewhere at $0 \leq z < 1$. Vanishing of the numerator at $z = 1$ does not pose a problem since $f'(z)$ diverges and tends to $(c - 1)(1 - z)^{-2}$ for $z = 1$, being positive in vicinity of $z = 1$ for $c > 1$ and negative for $c < 1$ due to the fact that the denominator vanishes even faster. Now we show that this function never changes its sign on $0 \leq z < 1$. Calculating the derivative

$$g'(z) = -c(c - 1)z^{c-2} + c(c - 1)z^{c-1} = -c(c - 1)z^{c-2}(1 - z)$$

we see that it is strictly positive for all $z < 1$ for $c < 1$ and strictly negative for $c > 1$. Therefore the bounds for the function $f(z)$ are given by its limiting values of 1 at $z = 0$ and c at $z = 1$. Therefore we have $A = \min(1, c^2)$ and $B = \max(1, c^2)$. Since for $1 > a + 2c$

$$\int_0^1 (1 - z)^{-a-2c} dz = \frac{1}{1 - a - 2c}$$

we get

$$\frac{\min(1, c^2)}{1 - a - 2c} \leq C \leq \frac{\max(1, c^2)}{1 - a - 2c}. \quad (\text{B.6})$$

Therefore, for $a + 2c < 1$ we have, for y small,

$$I_{a,b,c}(y) \simeq Cy^{1+a+2c} \quad (\text{B.7})$$

where the bounds for the constant C are given by Eq.(B.6).

For the opposite case $a + 2c > 1$ we have to use the other Pfaff transformation, Eq.(B.5), resulting in:

$$\begin{aligned} I_{a,b,c}(y) = & (1+y)^a \\ & \times \left[(1+y)^{2c} B(1, 1+b)_2 F_1(-a-2c, 1+b; 2+b; 1/(1+y)) \right. \\ & - 2(1+y)^c B(1+c, 1+b)_2 F_1(-a-c, 1+b; 2+b+c; 1/(1+y)) \\ & \left. + B(1+2c, 1+b)_2 F_1(-a, 1+b; 2+b+2c; 1/(1+y)) \right]. \end{aligned} \quad (\text{B.8})$$

Using the integral representation Eq.(B.2) again we find

$$\begin{aligned} I_{a,b,c}(y) = & (1+y)^a \int_0^1 \left[(1+y)^{2c} z^b \left(1 - \frac{z}{1+y} \right)^{a+2c} \right. \\ & - 2(1+y)^c z^b (1-z)^c \left(1 - \frac{z}{1+y} \right)^{a+c} \\ & \left. + z^b (1-z)^{2c} \left(1 - \frac{z}{1+y} \right)^a \right] dz. \end{aligned} \quad (\text{B.9})$$

Now we expand the expression in each term of the integrand up to second order in y . Using the fact that

$$(1+y)^\alpha \simeq 1 + \alpha y + \frac{\alpha(\alpha-1)}{2} y^2,$$

and

$$\begin{aligned} \left(1 - \frac{z}{1+y} \right)^\alpha & \simeq (1-z)^\alpha + \alpha(1-z)^{\alpha-1} zy \\ & + \frac{1}{2} \left[\alpha(\alpha-1)(1-z)^{\alpha-2} z^2 - 2\alpha(1-z)^{\alpha-1} z \right] y^2, \end{aligned}$$

as well as the definition of the Beta function

$$B(a, b) = \int_0^1 z^{a-1} (1-z)^{b-1} dz,$$

we find:

$$I_{a,b,c}(y) \simeq c^2 y^2 [B(1+b, 1+a+2c) + 2B(2+b, a+2c) + B(3+b, a+2c-1)].$$

The first two orders in y have canceled, so the leading term goes as y^2 . From the argument of the last Beta function it is clear, that the result only holds for $a+2c > 1$, i.e. exactly in the parameter range where Eq.(B.7) ceases to be applicable, and that the exponents are continuous at $a+2c = 1$. Rewriting the Beta functions as $B(a, b) = \Gamma(a)\Gamma(b)/\Gamma(a+b)$ and (repeatedly) using the identity $\Gamma(x+1) = x\Gamma(x)$ we find a compact representation of the sum of the three beta functions, namely

$$I_{a,b,c}(y) \simeq c^2 y^2 B(1+b, a+2c-1). \quad (\text{B.10})$$

In conclusion we have:

$$I_{a,b,c}(y) \simeq \begin{cases} C(a, c) y^{1+a+2c} & \text{for } a+2c < 1 \\ c^2 B(1+b, a+2c-1) y^2 & \text{for } a+2c > 1, \end{cases}$$

which is the Eq.(4.85) of the main text, with the bounds on a constant $C(a, c)$ given by Eq.(B.6).

List of Figures

2.1.	Comparison between the trajectories of the one dimensional Lévy flight and Lévy walk (for $\nu = 1$). Note that the jump length of the Lévy flight is independent of the waiting time.	4
2.2.	Comparison of a walker's motion for different values of η : The trajectories and change points remain the same, but the position measured at time t varies. For $\eta = 1$ the walker moves with constant speed and has some non-linear time dependence for $\eta > 1$. In the limits $\eta = 0$ and $\eta = \infty$ we replicate the time-coupled Lévy flight, where the two limits correspond to the walker jumping first and then waiting or waiting first and then jumping.	6
2.3.	Illustration of the path of a Lévy walker on the time axis. Each tick on the line represents a change time. The walker starts at $t = 0$ and is observed at time t during a final incomplete step described by the distribution $r(\mathbf{x}, t)$ after it has completed a series of steps, which is described by $C(\mathbf{x}, t)$	10
2.4.	Illustration of an aged Lévy walk on the time axis. Each tick on the line represents a change time. The walker starts at $-t_a$ and observation begins at $t = 0$. In the upper picture we see the case that the first observed change time is at $t' < t$, the probability of this event is given by F . From here walker performs a series of completed steps and a final incomplete step as in the ordinary case. The lower picture shows the case that the first change point is after the end of observation, i.e. the walker never stops during observation. The probability density of this event is given by s	11
4.1.	Values of α in the different regions of parameter space. Solid lines correspond to changes in the regime.	42
5.1.	The picture shows the asymptotic time dependence of the ensemble average $\langle x^2 \rangle \propto t^x$ in the ordinary Lévy walk. The thick solid lines correspond to the changes in time exponent while the hatchings indicate the type of diffusion. The dashed line corresponds to ballistic behavior and the dotted one to the Richardson law.	43
5.2.	Fit of the time dependence for the ordinary MSD in the case $\gamma = 0.6$, $\nu = 1.5$ and $\eta = 1.7$ ($\chi^2 = 0.01$).	45

5.3.	The panel shows the asymptotic behavior of the ensemble average $\langle x^2(t) \rangle$ for the Lévy walk in the limit of long aging times. The thick solid lines correspond to the changes in time-dependence while the hatchings represent the different types of diffusion.	46
5.4.	Fit of the aging time dependence for the aged MSD in the case $\gamma = 0.8$, $\nu = 1.1$ and $\eta = 1.1$ ($\chi^2 = 2.88$).	47
5.5.	Histograms of a Lévy walk with $\gamma = 0.6$, $\nu = 1.3$ and $\eta = 1.3$ at different points in time. The dashed line indicates the position a walker would have reached in a single step beginning at $t = 0$ and ending exactly at the time of the respective panel.	48
5.6.	Histograms of a Lévy walk with $\gamma = 0.6$, $\nu = 1.3$ and $\eta = 1.1$ at different points in time. The dashed line indicates the position a walker would have reached in a single step beginning at $t = 0$ and ending exactly at the time of the respective panel.	50
5.7.	Histograms of a Lévy walk with $\gamma = 0.6$, $\nu = 1.3$ and $\eta = 1.5$ at different points in time. The dashed line indicates the position a walker would have reached in a single step beginning at $t = 0$ and ending exactly at the time of the respective panel.	51
5.8.	Histograms of a Lévy walk with $\gamma = 0.6$, $\nu = 0.8$ and $\eta = 0.8$ at different points in time. The dashed line indicates the position a walker would have reached in a single step beginning at $t = 0$ and ending exactly at the time of the respective panel.	52
5.9.	Histograms of a Lévy walk with $\gamma = 1.2$, $\nu = 1.3$ and $\eta = 1.3$ at different points in time. The dashed line indicates the position a walker would have reached in a single step beginning at $t = 0$ and ending exactly at the time of the respective panel.	53
5.10.	Histograms of a Lévy walk with $\gamma = 1.2$, $\nu = 0.4$ and $\eta = 0.4$ at different points in time. The dashed line indicates the position a walker would have reached in a single step beginning at $t = 0$ and ending exactly at the time of the respective panel.	54
5.11.	Histograms of an aged Lévy walk with $\gamma = 0.6$, $\nu = 1.3$ and $\eta = 1.3$ and aging time $t_a = 10^5 t_0$ at different observation times. The dashed line indicates the position a walker would have reached in a single step beginning at $t = 0$ and ending exactly at the time of the respective panel. The dotted line indicates the displacement a step could archive during the observation, if it starts at $-t_a$ and ends at t	55
5.12.	Histograms of an aged Lévy walk with $\gamma = 1.1$, $\nu = 1.3$ and $\eta = 1.3$ and aging time $t_a = 2 \cdot 10^4 t_0$ at different observation times. The dashed line indicates the position a walker would have reached in a single step beginning at $t = 0$ and ending exactly at the time of the respective panel. The yellow line indicates the displacement a step could archive during the observation, if it starts at $-t_a$ and ends at t	56

5.13. Histograms of an aged Lévy walk with $\gamma = 0.6$, $\nu = 0.8$ and $\eta = 0.8$ and aging time $t_a = 10^5 t_0$ at different observation times. The dashed line indicates the position a walker would have reached in a single step beginning at $t = 0$ and ending exactly at the time of the respective panel. The yellow line indicates the displacement a step could archive during the observation, if it starts at $-t_a$ and ends at t	57
5.14. The time dependence of the probability density for different values of the parameters ν and γ is shown. Thick lines indicate the distinction between two different regimes.	58
5.15. The time dependence of the probability density for the parameter values $\gamma = 1.5$, $\nu = 0.8$ and $\eta = 0.8$ is shown. It is fitted with $f(x) = ax^b$ ($\chi^2 = 0.12$).	59
5.16. Comparison of the histogram obtained in a simulation with $\gamma = 0.6$, $\nu = 0.8$ and $\eta = 1$ with the corresponding rescaled semi-analytic result for $\alpha = 0.8$	60
5.17. Comparison of the histogram obtained in a simulation with $\gamma = 1.2$, $\nu = 0.4$ and $\eta = 0.4$ with the corresponding rescaled analytic result for $\alpha = 0.5$	61

List of Tables

4.1. Leading terms of the marginal moments of C and r in the Laplace domain for different parameter ranges.	24
4.2. Results for F_0 and F_2 in the Laplace domain as well as s_2 in the time domain for different parameter ranges in the case of weak aging $t \gg t_a$. Dimensionless prefactors are omitted.	33
4.3. Results for F_0 and F_2 in the Laplace domain as well as s_2 in the time domain for different parameter ranges in the case of long aging times $t_a \gg t \gg t_0$. Dimensionless prefactors are omitted.	37
4.4. Asymptotic behavior of the contributions to the MSD for $\gamma < 1$ in the limit $t_a \gg t \gg t_0$. All dimensionless prefactors are omitted. The dominant terms are highlighted in boldface.	38
4.5. Asymptotic behavior of the contributions to the MSD for $\gamma > 1$ in the limit $t_a \gg t \gg t_0$. All dimensionless prefactors are omitted. The dominant terms are highlighted in boldface.	38

Bibliography

- [1] XU, Q ; FENG, L ; SHA, R ; SEEMAN, NC ; CHAIKIN, PM: Subdiffusion of a Sticky Particle on a Surface. In: *Phys. Rev. Lett.* 106 (2011), Jun, 228102. <http://dx.doi.org/10.1103/PhysRevLett.106.228102>. – DOI 10.1103/PhysRevLett.106.228102
- [2] SAGI, Y ; BROOK, M ; ALMOG, I ; DAVIDSON, N: Observation of Anomalous Diffusion and Fractional Self-Similarity in One Dimension. In: *Phys. Rev. Lett.* 108 (2012), Mar, 093002. <http://dx.doi.org/10.1103/PhysRevLett.108.093002>. – DOI 10.1103/PhysRevLett.108.093002
- [3] MARTY, G ; DAUCHOT, O: Subdiffusion and Cage Effect in a Sheared Granular Material. In: *Phys. Rev. Lett.* 94 (2005), Jan, 015701. <http://dx.doi.org/10.1103/PhysRevLett.94.015701>. – DOI 10.1103/PhysRevLett.94.015701
- [4] AMBLARD, F ; MAGGS, AC ; YURKE, B ; PARGELLIS, A. N. ; LEIBLER, S.: Subdiffusion and Anomalous Local Viscoelasticity in Actin Networks. In: *Phys. Rev. Lett.* 77 (1996), Nov, 4470–4473. <http://dx.doi.org/10.1103/PhysRevLett.77.4470>. – DOI 10.1103/PhysRevLett.77.4470
- [5] SHLESINGER, MF ; WEST, BJ ; KLAFTER, J: Lévy dynamics of enhanced diffusion: Application to turbulence. In: *Physical Review Letters* 58 (1987), Nr. 11, S. 1100
- [6] RICHARDSON, LF: Atmospheric diffusion shown on a distance-neighbour graph. In: *Proceedings of the Royal Society of London. Series A, Containing Papers of a Mathematical and Physical Character* 110 (1926), Nr. 756, S. 709–737
- [7] ZABURDAEV, V ; DENISOV, S ; KLAFTER, J: Lévy walks. In: *Reviews of Modern Physics* 87 (2015), Nr. 2, S. 483
- [8] MARKSTEINER, S ; ELLINGER, K ; ZOLLER, P: Anomalous diffusion and Lévy walks in optical lattices. In: *Physical Review A* 53 (1996), Nr. 5, S. 3409
- [9] JUNG, Y ; BARKAI, E ; SILBEY, RJ: Lineshape theory and photon counting statistics for blinking quantum dots: a Lévy walk process. In: *Chemical Physics* 284 (2002), Nr. 1-2, S. 181–194
- [10] ZABURDAEV, V ; DENISOV, S ; HÄNGGI, P: Perturbation spreading in many-particle systems: a random walk approach. In: *Physical review letters* 106 (2011), Nr. 18, S. 180601

- [11] KOROBKOVA, E ; EMONET, T ; VILAR, JMG ; SHIMIZU, TS ; CLUZEL, P: From molecular noise to behavioural variability in a single bacterium. In: *Nature* 428 (2004), Nr. 6982, S. 574
- [12] ALBERS, T ; RADONS, G: Exact results for the nonergodicity of d-dimensional generalized levy walks. In: *Physical review letters* 120 (2018), Nr. 10, S. 104501
- [13] BENKADDA, S ; ZASLAVSKY, GM: *Chaos, Kinetics and Nonlinear Dynamics in Fluids and Plasmas: Proceedings of a Workshop Held in Carry-Le Rouet, France, 16–21 June 1997*. Bd. 511. Springer Science & Business Media, 1998
- [14] SCHULZ-BALDES, H: Anomalous Drude Model. In: *Physical review letters* 78 (1997), Nr. 11, S. 2176
- [15] BOTHE, M ; SAGUES, F ; SOKOLOV, IM: Mean squared displacement in a generalized Lévy walk model. In: *Phys. Rev. E* 100 (2019), Jul, 012117. <http://dx.doi.org/10.1103/PhysRevE.100.012117>. – DOI 10.1103/PhysRevE.100.012117
- [16] KLAFTER, J ; SOKOLOV, IM: *First steps in random walks: from tools to applications*. Oxford University Press, 2011
- [17] BARKAI, E: Aging in Subdiffusion Generated by a Deterministic Dynamical System. In: *Phys. Rev. Lett.* 90 (2003), Mar, 104101. <http://dx.doi.org/10.1103/PhysRevLett.90.104101>. – DOI 10.1103/PhysRevLett.90.104101
- [18] BARKAI, E ; CHENG, Y-C: Aging continuous time random walks. In: *The Journal of chemical physics* 118 (2003), Nr. 14, S. 6167–6178
- [19] KLAGES, R ; RADONS, G ; SOKOLOV, IM: *Anomalous transport*. Wiley Online Library, 2008
- [20] BROKMAN, X ; HERMIER, J-P ; MESSIN, G ; DESBIOLLES, P ; BOUCHAUD, J-P ; DAHAN, M: Statistical Aging and Nonergodicity in the Fluorescence of Single Nanocrystals. In: *Phys. Rev. Lett.* 90 (2003), Mar, 120601. <http://dx.doi.org/10.1103/PhysRevLett.90.120601>. – DOI 10.1103/PhysRevLett.90.120601
- [21] MAGDZIARZ, M ; SCHEFFLER, H-P ; STRAKA, P ; ZEBROWSKI, P: Limit theorems and governing equations for Lévy walks. In: *Stochastic Processes and their Applications* 125 (2015), Nr. 11, S. 4021–4038
- [22] MAGDZIARZ, M ; ZORAWIK, T: Method of calculating densities for isotropic ballistic Lévy walks. In: *Communications in Nonlinear Science and Numerical Simulation* 48 (2017), S. 462–473
- [23] TALBOT, A: The accurate numerical inversion of Laplace transforms. In: *IMA Journal of Applied Mathematics* 23 (1979), Nr. 1, S. 97–120

- [24] ABATE, J ; VALKÓ, PP: Multi-precision Laplace transform inversion. In: *International Journal for Numerical Methods in Engineering* 60 (2004), Nr. 5, S. 979–993
- [25] MARSAGLIA, G u. a.: Xorshift rngs. In: *Journal of Statistical Software* 8 (2003), Nr. 14, S. 1–6
- [26] PRUDNIKOV, AP: *Yu. A. Brychkov, and OI Marichev. 1986. Integrals and Series, Vol. 1. Elementary Functions.* 1986
- [27] MAGDZIARZ, M ; ZORAWIK, T: Aging ballistic Lévy walks. In: *Physical Review E* 95 (2017), Nr. 2, S. 022126
- [28] FROEMBERG, D ; BARKAI, E: Time-averaged Einstein relation and fluctuating diffusivities for the Lévy walk. In: *Physical Review E* 87 (2013), Nr. 3, S. 030104
- [29] MATHAI, AM ; SAXENA, RK ; HAUBOLD, HJ: *The H-function: theory and applications.* Springer Science & Business Media, 2009
- [30] PENSON, KA ; GÓRSKA, K: Exact and explicit probability densities for one-sided Lévy stable distributions. In: *Physical review letters* 105 (2010), Nr. 21, S. 210604
- [31] BURIONI, R ; GRADENIGO, G ; SARRACINO, A ; VEZZANI, A ; VULPIANI, A: Rare events and scaling properties in field-induced anomalous dynamics. In: *Journal of Statistical Mechanics: Theory and Experiment* 2013 (2013), Nr. 09, S. P09022
- [32] BURIONI, R ; GRADENIGO, G ; SARRACINO, A ; VEZZANI, A ; VULPIANI, A: Scaling properties of field-induced superdiffusion in continuous time random walks. In: *Communications in Theoretical Physics* 62 (2014), Nr. 4, S. 514

Acknowledgement

I am especially grateful to Prof. Sokolov, who provided me with this topic, guided and helped me throughout the entire process and was always very generous with his time when it came to my questions.

I would also like to thank Francesc Sagues for the great discussions and his meticulous proofreading of the calculations.

Selbstständigkeitserklärung

Hiermit versichere ich, dass ich die vorliegende Arbeit selbständig verfasst und keine anderen als die angegebenen Quellen und Hilfsmittel verwendet habe.

Ort, Datum

Unterschrift